

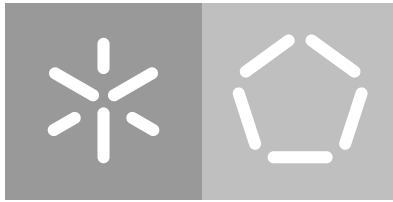
Universidade do Minho
Escola de Engenharia
Departamento de Informática

Jaime Pereira Santos

Quantum Random Walks

Simulations and physical realizations

September 2021



Universidade do Minho
Escola de Engenharia
Departamento de Informática

Jaime Pereira Santos

Quantum Random Walks

Simulations and physical realizations

Master dissertation
Integrated Master's in Physics Engineering

Dissertation supervised by
Luís Barbosa
Bruno Chagas

September 2021

COPYRIGHT AND TERMS OF USE

This is an academic work that can be used by third parties as long as good practices are respected as well as internationally accepted rules concerning copyright and related rights. Thereby, this work can be used under the terms set out in the license below. If one needs permission to work under a different set of conditions not provided by the indicated license, one must contact the author, through the University of Minho *RepositoriUM*.



Atribuição
CC BY |

<https://creativecommons.org/licenses/by/4.0/>

STATEMENT OF INTEGRITY

I hereby declare having conducted this academic work with integrity. I confirm that I have not used plagiarism or any form of undue use of information or falsification of results along the process leading to its elaboration. I further declare that I have fully acknowledged the Code of Ethical Conduct of the University of Minho.

ACKNOWLEDGEMENTS

I would like to express my gratitude to my supervisor prof. Luís Barbosa, for all of the opportunities, support and patience throughout the entirety of my Masters degree; to my co-supervisor Bruno Chagas, for the countless hours dedicated to the development of this dissertation and invaluable advice.

I would also like to thank my family, especially my parents, for their unconditional support throughout all my life.

A very special thank you to my girlfriend, Cláudia Vieira, for her love and encouragement and also for keeping me grounded in these trying times.

Finally, this dissertation was financed by the ERDF – European Regional Development Fund through the Operational Programme for Competitiveness and Internationalization - COMPETE 2020 Programme and by National Funds through the Portuguese funding agency, FCT - Fundação para a Ciência e a Tecnologia, within project POCI-01-0145-FEDER-030947.

ABSTRACT

Quantum computing is an emergent field that brings together Quantum Mechanics, Computer Science and Information Theory, which promises improvements to classical algorithms such as simulation of quantum systems, cryptography, data base searching and many others. Among these algorithms, quantum walks may provide a quadratic speed up when compared to their classical counterparts, allowing improvements to applications such as element distinctness, searching problems, matrix product verification and hitting times in graphs. The present work offers a general theoretical overview, simulation and circuit implementation of the coined, staggered and continuous-time quantum walk models. The first two chapters of this thesis are dedicated to the definition of the theoretical framework, simulation in Python and comparison of the aforementioned quantum walk models for the simple case of the dynamics in a line graph and for the search algorithm in a complete graph. This is then used as a benchmark for the final chapter, devoted to building and testing the circuits corresponding to models mentioned above in IBM's Qiskit. A main contribution of this dissertation concerns the circulant graph approach to diagonal operators for continuous-time quantum walks.

Keywords: Quantum Computing Quantum Walks Python Qiskit

RESUMO

A computação quântica é uma área emergente, que junta os campos de Mecânica Quântica, Ciências da Computação e Teoria da Informação, com a promessa de melhoramentos a algoritmos clássicos tais como a simulação de sistemas quânticos, criptografia, busca em base de dados, e outros. Entre estes algoritmos, as caminhadas quânticas surgem com um ganho quadrático de complexidade em comparação às caminhadas clássicas, possibilitando melhor desempenho em aplicações como distinção de elementos, problemas de busca, verificação de produtos de matrizes e tempos de alcance em grafos. O trabalho atual oferece uma visão geral de um ponto de vista teórico, de simulação e de implementação de circuitos, relativos aos modelos de caminhadas quânticas com moeda, escalonadas e contínuas no tempo. Os primeiros dois capítulos desta tese são dedicados à definição da estrutura teórica, simulação em Python e comparação dos modelos supracitados, para o caso simples da dinâmica na linha, e para o problema de busca num grafo completo. Isto será então utilizado como referência para o capítulo final, dedicado à construção e teste dos circuitos correspondentes aos modelos supracitados. Uma contribuição principal desta dissertação diz respeito à abordagem de grafos circulantes para realização de caminhadas quânticas contínuas no tempo.

Palavras-Chave: Computação Quântica Caminhadas Quânticas Python Qiskit

CONTENTS

1	INTRODUCTION	1
1.1	Brief History of Quantum Computing	1
1.2	Classical and Quantum Walks	4
1.3	State of the Art on Quantum Walk Implementations	6
1.4	Objectives, Contributions and Structure	8
2	QUANTUM WALKS	10
2.1	Classical Random Walk	10
2.2	Coined Quantum Walk	12
2.3	Staggered Quantum Walk	17
2.4	Continuous-Time Quantum Walk	20
3	SEARCHING PROBLEMS	24
3.1	Grover's Algorithm	24
3.1.1	One marked element	26
3.1.2	Multiple marked elements	28
3.1.3	Single-Shot Grover	30
3.2	Coined Quantum Walk	31
3.3	Staggered Quantum Walk	33
3.4	Continuous-Time Quantum Walk	35
4	IMPLEMENTATIONS AND APPLICATIONS	39
4.1	Coined Quantum Walk	40
4.2	Staggered Quantum Walk	43
4.3	Continuous-Time Quantum Walk	46
4.4	Implementing Search Algorithms in Qiskit	52
4.4.1	Grover's Algorithm	52
4.4.2	Searching with a Coined Quantum Walk	55
4.4.3	Searching with a Staggered Quantum Walk	58
4.4.4	Searching with a Continuous-Time Quantum Walk	61
5	DISCUSSIONS AND CONCLUSION	65
A	SUPPORT MATERIAL	75
A.1	The Postulates of Quantum Mechanics	75
A.2	Quantum Fourier Transform	79

LIST OF FIGURES

Figure 1	Probability distribution for the classical random walk on a line, after 72, 180 and 450 steps, running 300000 experiments for each number of steps, with starting position on vertex 0.	11
Figure 2	Standard deviation after 200 steps for the quantum walk in blue, and the classical random walk in red.	14
Figure 3	Probability distribution for the coined quantum walk on a line, after 32, 64 and 128 steps, with initial condition $ \psi(0)\rangle = 0\rangle x = 0\rangle$ and the Hadamard coin.	14
Figure 4	Probability distribution for the coined quantum walk on a line, after 32, 64 and 128 steps, with initial condition $ \psi(0)\rangle = 1\rangle x = 0\rangle$ and the Hadamard coin.	15
Figure 5	Probability distribution for the coined quantum walk on a line, after 32, 64 and 128 steps, with initial condition $ \psi(0)\rangle = \frac{ 0\rangle + i 1\rangle}{\sqrt{2}} x = 0\rangle$ and the Hadamard coin.	16
Figure 6	Tessellation of a line graph.	18
Figure 7	Probability distribution for the staggered quantum walk on a line after 50 steps, with initial condition $ \psi(0)\rangle = \frac{ 0\rangle + 1\rangle}{\sqrt{2}}$, for multiple values of θ .	18
Figure 8	Probability distributions for the staggered quantum walk on a line after 50 steps, for different initial conditions.	19
Figure 9	Probability distribution for the continuous-time quantum walk on a line, at $t = 40, 80$ and 120 , with initial condition $ \psi(0)\rangle = 0\rangle$ and $\gamma = \frac{1}{2\sqrt{2}}$.	21
Figure 10	Probability distribution for the continuous-time quantum walk on a line, at $t = 100$, with initial condition $ \psi(0)\rangle = \frac{ 0\rangle + 1\rangle}{\sqrt{2}}$, for multiple values of γ .	22
Figure 11	Probability of one marked element in the Grover search, as a function of the number of steps, for $N = 32, 64, 128$ and 256 .	27
Figure 12	Probability of two marked elements in the Grover search, as a function of the number of steps, for $N = 32, 64, 128$ and 256 .	29
Figure 13	Total probability of marked elements in the Grover search, as a function of the number of marked elements, for 1 step, with $N = 32, 64, 128$ and 256 .	30

Figure 14	Probability of one marked element in the coined quantum walk search, as a function of the number of steps, for complete graphs of size $N = 16, 32$ and 64 .	32
Figure 15	Maximum probability of the marked element as a function of the value of θ plotted from 0 to π , for complete graphs of size $N = 64, 128$ and 256 .	34
Figure 16	Probability of one marked element in the staggered quantum walk search, as a function of the number of steps, for complete graphs of size $N = 16, 32$ and 64 .	35
Figure 17	Value of the difference between the largest eigenvalue and the second largest plotted as a function of γN , for $N = 512$.	36
Figure 18	Probability of one marked element in the continuous quantum walk search, as a function of the number of steps, for complete graphs of size $N = 16, 32$ and 64 .	37
Figure 19	General circuits of the components of the shift operator for the coined quantum walk.	40
Figure 20	General circuit for the coined quantum walk.	41
Figure 21	Qiskit circuit for the coined quantum walk, for a line graph of size $N = 8$ and initial condition $ \psi_0\rangle = 4\rangle$, with 3 steps and the Hadamard coin.	41
Figure 22	Qiskit circuits of the components of the shift operator for the coined quantum walk, for a line graph of size $N = 8$.	41
Figure 23	Probability distributions of the coined quantum walk for several steps in a line graph of size $N = 8$. The blue bar plot represents a circuit run in the QASM simulator, and the orange bar plot on IBM's Toronto backend.	42
Figure 24	General circuit for the staggered quantum walk.	44
Figure 25	Qiskit circuit for the staggered quantum walk, for a line graph of size $N = 8$ and initial condition $ \psi_0\rangle = 4\rangle$, with 3 steps.	45
Figure 26	Probability distributions of the staggered quantum walk for several steps in a line graph of size $N = 8$. The blue bar plot represents a circuit run in the QASM simulator, and the orange bar plot on IBM's Toronto backend.	45
Figure 27	General circuit for the continuous-time quantum walk.	48
Figure 28	Qiskit circuit for the continuous-time quantum walk, for a line graph of size $N = 8$ and initial condition $ \psi_0\rangle = 4\rangle$, for time t .	48
Figure 29	Qiskit circuit of the quantum Fourier transform for a line graph of size $N = 8$.	48

Figure 30	Qiskit circuit of the diagonal operator associated with the adjacency matrix, for a line graph of size $N = 8$.	49
Figure 31	Probability distributions of the continuous-time quantum walk for several steps in a line graph of size $N = 8$. The blue bar plot represents a circuit run in the QASM simulator, and the orange bar plot on IBM's Toronto backend.	49
Figure 32	Circulant graphs G_k for $N = 8$ elements.	50
Figure 33	General circuit for the Grover search.	53
Figure 34	Qiskit circuit for the Grover algorithm, for a search space of size $N = 8$ and 3 steps.	53
Figure 35	Qiskit circuit of the diagonal oracle operator for a search space of size $N = 8$ and marked element $ m\rangle = 4\rangle$.	53
Figure 36	Qiskit circuit of the diagonal Grover diffusion operator for a search space of size $N = 8$.	54
Figure 37	Probability distributions of the Grover search algorithm for several steps, in a search space of size $N = 8$. The blue bar plot represents a circuit run in the QASM simulator, and the orange bar plot on IBM's Toronto backend.	54
Figure 38	General circuit for the search problem using the coined quantum walk model.	55
Figure 39	Qiskit circuit for the search problem using the coined quantum walk model, for a complete graph of size $N = 8$ and with 5 steps.	55
Figure 40	Qiskit circuit of the diagonal oracle operator in the coined quantum walk search problem, for a complete graph of size $N = 8$, with marked element $ m\rangle = 4\rangle$.	56
Figure 41	Qiskit circuit of the diagonal diffusion operator in the coined quantum walk search problem, for a complete graph of size $N = 8$.	56
Figure 42	Qiskit circuit of the flip-flop shift operator in the coined quantum walk search problem, for a complete graph of size $N = 8$.	57
Figure 43	Probability distributions of the coined quantum walk search problem for several steps, in a complete graph of size $N = 8$. The blue bar plot represents a circuit run in the QASM simulator, and the orange bar plot on IBM's Toronto backend.	57
Figure 44	General circuit for the search problem using the staggered quantum walk model.	58
Figure 45	Qiskit circuit for the search problem using the staggered quantum walk model, for a complete graph of size $N = 8$, with 3 steps and a value of $\theta = \frac{\pi}{2}$.	59

- Figure 46 Qiskit circuit of the diagonal diffusion operator in the staggered quantum walk search problem, for a complete graph of size $N = 8$ and a value of $\theta = \frac{\pi}{2}$. 59
- Figure 47 Probability distributions of the staggered quantum walk search problem for several steps, in a complete graph of size $N = 8$. The blue bar plot represents a circuit run in the QASM simulator, and the orange bar plot on IBM's Toronto backend. 60
- Figure 48 General circuit for the search problem using the continuous-time quantum walk model. 62
- Figure 49 Qiskit circuit for the search problem using the continuous-time quantum walk model, for a complete graph of size $N = 8$, time t , a value of $\gamma = \frac{1}{8}$ and a Trotter number $r = 1$. 62
- Figure 50 Qiskit circuit of the diagonal oracle operator in the continuous-time quantum walk search problem, for a complete graph of size $N = 8$, marked element $|m\rangle = |4\rangle$ and time $t = \frac{\pi}{2}\sqrt{8}$. 62
- Figure 51 Qiskit circuit of the diagonal operator associated with the adjacency matrix in the continuous-time quantum walk search problem, for a complete graph of size $N = 8$, marked element $|m\rangle = |4\rangle$, time $t = \frac{\pi}{2}\sqrt{8}$ and $\gamma = \frac{1}{8}$. 63
- Figure 52 Probability distributions of the continuous-time quantum walk search problem for several time intervals, in a complete graph of size $N = 8$. The blue bar plot represents a circuit run in the QASM simulator, and the orange bar plot on IBM's Toronto backend. 63
- Figure 53 General circuit for the quantum Fourier transform. 80

LIST OF TABLES

Table 1	Fidelity of quantum state with $N=4$, backend <i>Toronto</i> , and $t=1$.	51
Table 2	Fidelity of quantum state with $N=8$, backend <i>Toronto</i> , and $t=1$.	51
Table 3	Fidelity of quantum state with $N=16$, backend <i>Toronto</i> , and $t=1$.	51

INTRODUCTION

This dissertation focuses on the study of quantum random walks and their implementation. Its structure and contributions are detailed in section 1.4. Before that, however, the whole area of work is put in context along sections 1.1 to 1.3. The first one starts from the very beginning through a brief history of quantum computation, which aims at motivating a discussion on classical and quantum random walks in section 1.2. Finally, section 1.3 presents the the state of the art concerning the implementation of quantum walks as a background for the dissertation's contributions.

1.1 BRIEF HISTORY OF QUANTUM COMPUTING

The modern understanding of computer science was firstly put forward by Turing (1936) where he developed the abstract concept of what is now called a *Turing machine*. These machines are the mathematical foundation of programmable computers, and Turing showed that there is a *Universal Turing Machine* that can be used to simulate any other Turing Machine. This means that if an algorithm can be executed in any piece of hardware, then there is a Universal Turing Machine that can accomplish the same task. This is known as the *Church-Turing thesis*, which connects the concept of what classes of algorithms can be run in some physical device with the mathematical framework of a Universal Turing Machine.

The paper published by Turing set in motion a series of events which led to the rapid advancement of electronic computers and computer science. One of the earliest theoretical models developed by John von Neumann (later published in von Neumann (1993)), showed how to assemble all the necessary parts to create a computer with all the capabilities of a Universal Turing Machine. The true explosion of innovation in this field came after the invention of the transistor in 1947 by John Bardeen and Walter Brattain. The creation of the transistor led to an unprecedented growth quantified by Moore (1965), known as *Moore's law*, stating that computer power will double with constant cost approximately every two years. Moore's law has roughly held true throughout the decades, by the ever increasing miniaturization of the transistor technology. However, conventional fabrication methods run

into a problem of scale, as quantum effects begin to interfere more and more as the size of the devices becomes smaller.

Feynman (1959) recognized such a miniaturization was the way forward as computational resources, and even predicted the problems quantum effects presented to a classical computer. With an amazing stroke of insight, Feynman imagined that these effects could be exploited given the right computational paradigm. Quantum computing begins to take form in later work developed by Benioff (1980), where the earliest quantum mechanical model of a computer was described. In this paper, Benioff showed that a computer working under the laws of quantum mechanics could be used to express a Schrödinger equation description of a Turing machine. Shortly after, Feynman (1982) pointed out that simulating quantum systems on classical computers is inefficient, and suggested using quantum computers for this purpose. Additional work in the following decade further explored this idea and showed that there are systems that quantum computers can simulate, which have no known efficient simulation on a classical computer. Even today this continues to be one of the most promising fields in quantum computing.

Driven by the work of Turing, Deutsch (1985) questioned if a stronger version of the Church-Turing thesis could be derived from the laws of physics. The strong Church-Turing thesis states that any algorithmic process can be simulated efficiently using a probabilistic Turing machine, and Deutsch was set to define some device that could efficiently simulate an arbitrary physical system. Whether Deutsch's formulation of a Universal Quantum Computer is sufficient for this purpose is still an open question. What he accomplished, however, was a challenge to the strong Church-Turing thesis by suggesting that there are tasks a quantum computer can accomplish efficiently that a probabilistic Turing machine cannot. Deutsch and Jozsa (1992) present an example of a quantum algorithm that is exponentially faster than a classical counterpart, the *Deutsch-Jozsa algorithm* that determines if a function is constant or balanced. Even though of little practical use, this is one of the first examples of possible advantages a quantum computer may have over a classical one.

Even though the Deutsch-Jozsa algorithm might not have real world applications, it led to further research on finding other such types of algorithms. Shor (1994a) showed that the problem of finding prime factors of an integer and the *discrete logarithm* problem can be efficiently solved by a quantum computer. This brought a lot of interest to quantum computing, since both of these problems have real world applications and no efficient classical solution was/is known. Furthermore, most modern popular algorithms used for cryptography rely on the fact that the integer factorization or discrete logarithm problems are not solvable in time that grows polynomially with the size of the problem. Since this is no longer the case, a new field has emerged called *post-quantum cryptography*, whose purpose is to find suitable classical protocols for cryptography that cannot be efficiently broken by quantum computing.

A more modest, but very relevant advantage was presented by Grover (1996) in the form of a quantum algorithm able to speed up unstructured database searches quadratically. Even though it's not an exponential improvement like Shor's algorithm, search-based algorithms are useful in many contexts, so even a "small" quadratic gain generated a lot of interest.

Contemporary to computer science, information theory is another field very relevant to this topic. Shannon (1948) revolutionized how communication and information are understood. In his paper, Shannon was interested in defining what resources are required to send information over a communication channel and how to reliably send that information mitigating the effects of noise. This led to the discovery of the two fundamental theorems of information theory. Firstly, Shannon's *noiseless channel coding theorem* specifies what resources are needed to store information sent from a source. Secondly, the *noisy channel coding theorem*, specifies how much information can be sent through a channel subject to noise. Even though Shannon's second theorem does not define any specific methodology to reduce noise, it sets an upper limit on how much noise can be mitigated through said methodology. These are known as *error-correcting codes* and research has developed better and better codes that get closer and closer to Shannon's limit. They are used wherever there is a need to store or transmit information.

Similar progress was made in quantum information theory. Schumacher (1995) developed a quantum version of Shannon's noiseless coding theorem, where he defined a *quantum bit* as a physical resource. There is no analogue for the second Shannon theorem, but that didn't stop the development of quantum error-correcting theory. For example, Calderbank and Shor (1996) and Steane (1996) proposed an important class of quantum error-correcting codes known as CSS.

Error-correcting was designed to protect quantum states, but another discovery by Bennett and Wiesner (1992) showed another interesting aspect of quantum information when transmitting classical information through a quantum channel. They explained how to send two classical bits of information using only one qubit, in a phenomenon known as *superdense coding*.

Another interesting application of quantum information is in the field of cryptography. Wiesner (1983) showed how quantum mechanics could be used to make sure that a information sent could not be interfered with without destroying it. Building on this work, Bennett and Brassard (1984) proposed a quantum key distribution protocol between sender and receiver that could not be spied upon without notice. Many other protocols have since been proposed and experimental prototypes developed.

Finally, another interesting field within quantum computation is based on the concept of *distributed quantum computation*. Quantum clusters show promise since they require exponentially less communication to solve certain problems, such as modeling quantum systems, but are still in their infancy due to technical restrictions. There has been an increasing

international interest in taking advantage of these systems to build a *quantum internet* which promises better and safer transmission of information, but there are still many technological improvements to be made before this becomes a mainstream reality.

1.2 CLASSICAL AND QUANTUM WALKS

The Church-Turing thesis, that states that any algorithmic process can be simulated efficiently using a Turing Machine, was challenged by Solovay and Strassen (1977) where they presented what is known as the *Solovay-Strassen primality test*. They showed that it is possible to test whether an integer is prime or composite using a randomized algorithm. The implication is that, because of the randomness, the Solovay-Strassen primality test does not determine with certainty whether an integer is prime or composite, rather it computes that a number is *probably* prime or else *certainly* composite. This is of significance since no deterministic test for primality was known at the time¹, meaning that this was an example of a class of problems that could not be efficiently solved by a conventional deterministic Turing Machine.

This led to a modification of the Church-Turing thesis, now stating that any algorithm can be simulated efficiently using a *probabilistic* Turing machine. The discovery of more instances of such algorithms followed, Motwani and Raghavan (1995) and Papadimitriou (1994) show several problems that can be solved based on randomized algorithms. For example, the *Quicksort* algorithm, developed by Hoare (1961), has a high probability of finishing in $O(n \log n)$. In contrast to many deterministic algorithms that require $O(n^2)$ time. They also show algorithms that take advantage of *Markov chains* and the *Monte Carlo method*. The volume of a convex body, proposed by Dyer et al. (1991), can be estimated by a randomized algorithm in polynomial time; the permanent of a nonnegative entry matrix can also be approximately calculated in probabilistic polynomial time as was shown by Jerrum et al. (2004) and the *k-SAT* and satisfiability with restrictions problem by Schöning (1999).

Random walks, as the name suggests, belong to this class of algorithms. Pearson (1905) coined the term random walk, and they can be described as path consisting of a succession of steps determined by a stochastic process, over a mathematical space. They are a special case of *Markov chains*, which are stochastic processes that assume discrete values and whose next state is dictated by a deterministic or random rule based only on the current state. This is a useful framework, since it can be used to explain the behaviour of systems across many fields, from the Brownian movement of particles moving through a gas, to the price of a fluctuating stock as shown by Cootner (1967).

¹ Work by Agrawal et al. (2002) has since found a general, polynomial, deterministic, and unconditional primality proving algorithm.

The quantum analogue of the random walk was firstly developed by Aharonov et al. (1993), where they defined the *coined quantum random walk*. This model consists of a walker and a coin that determines the movement of the walker, which are both quantum systems where time is a discrete variable dictated by the successive quantum coin flips and shifts in position. Nayak and Vishwanath (2000) and Aharonov et al. (2001) present the first analyses of the quantum walk on a graph described by a line. Further work by Inui et al. (2003) studies the behaviour of the walk on grids and Aharonov et al. (2001) on general regular graphs. The first algorithmic applications appear in the work of Shenvi et al. (2003) where they constructed a search problem based on the quantum random walk, and Ambainis (2007) applied it to the element distinction problem. On a more theoretical note, Konno (2002) demonstrated how the classical and quantum models of the random walk on the line differ, and Grimmett et al. (2003) generalized this to higher dimensions. Lovett et al. (2010) demonstrated that any quantum algorithm can be reformulated as a discrete time quantum walk algorithm, effectively showing that this model can be used for universal quantum computation.

A different model for quantum random walks emerged from the work of Farhi and Gutmann (1998), where a different way of computing a search problem was presented. They showed that evolving a system in time between an initial and final Hamiltonian is analogous to the Grover algorithm, but continuous in time. Farhi et al. (2000) revised their work, now known as an adiabatic evolution, to solve Boolean *sat* problems. Childs and Goldstone (2004) formulated a model of a quantum walk in terms of adiabatic evolution, known as *continuous time quantum walk* or *adiabatic quantum walk*. Aharonov et al. (2007) showed that any quantum algorithm can be efficiently simulated using adiabatic evolution, meaning that it is polynomially equivalent to the conventional quantum computation model. Further work by Childs (2009) showed that this model is indeed universal. The main difference between these two quantum walk models lies on the fact that in the discrete case, the system evolves with the flipping of a coin and subsequent movement of the walker, whilst in the adiabatic case the system evolves smoothly in time.

Yet another way of thinking about quantum walks was announced by Szegedy (2004), where he describes a discrete model based on Markov chain random walks. At the foundation of this model is the duplication of a graph, a process by which a bipartite graph is created. Magniez et al. (2007) show how to use this walk for triangle detection in an undirected graph. Magniez et al. (2006) proposed a search problem, which takes advantage of ergodicity and symmetry properties of Markov chains, with quadratic gain compared to classical algorithms. Problems like element distinctness, matrix product verification and others were formulated within this framework by Santha (2008). Further work by Portugal (2015) established a connection between the coined and Szegedy's quantum walk, by defining a model that encompasses and expands the latter.

Patel et al. (2005) pointed that, at the time, there was confusion surrounding the scaling behaviour of discrete and adiabatic quantum walk algorithms. They argued that this was because the former model used a coin, which is an extra resource, and the latter didn't. So, in an attempt to resolve this confusion, they showed that a discrete time quantum walk could be constructed without the use of a coin. A new way of thinking about quantum walks came with the development of the methods behind the construction of evolution operators, by Falk (2013), introducing the concept of *tessellations*, based on local diffusion operators. Portugal et al. (2015) studied this model applied to a line graph. Further work by Portugal et al. (2016) formalized this approach naming it *staggered quantum walk*, and showed instances where the Szegedy quantum walk is equivalent. This suggests that this is a more general model, being able to describe other discrete-time quantum walks. Portugal et al. (2017) delved deeper into this topic, adding Hamiltonians to the model, and Portugal and Fernandes (2017) shows how this can be instanced as a search problem in a grid. Finally, Coutinho and Portugal (2018) analyze how a continuous-time quantum walk can be cast into this discrete model and Moqadam et al. (2017) show a possible physical implementation of this walk.

1.3 STATE OF THE ART ON QUANTUM WALK IMPLEMENTATIONS

One of the earliest works on a more computational approach to quantum random walks was by Marquezino and Portugal (2008), where they created a general simulator for discrete-time quantum walks on one- and two-dimensional lattices. They argued that this framework allowed researchers to focus more on the mathematical aspect of quantum walks, instead of the specific numerical implementations. Further work on these lattices was later presented by Sawerwain and Gielerek (2010), where they studied the simulation of quantum walks by taking advantage of the GPU and CUDA technology. Another interesting program for simulating discrete-time quantum walks came with the work of Berry et al. (2011). This package allows for direct simulation of these walks, and visualization of the time-evolution on arbitrary undirected graphs. It also allowed for plotting of continuous-time quantum walks, provided the data was provided externally. There are, however, direct simulators of continuous-time quantum walks, the earliest being by Izaac and Wang (2015). Their distributed memory software claims to be able to perform efficient simulation of multi-particle continuous-time quantum walk based systems, on *High Performance Computing* platforms. Falloon et al. (2017) provide a *Mathematica* package that implements a simulator of *Quantum Stochastic Walks*, which are a generalization of the continuous-time model. These walks incorporate both coherent and incoherent dynamics, which means that quantum stochastic walks can be instantiated as both quantum walks and classical random walks. What this paper then provides is a way of implementing quantum walks on directed graphs, opening the door to applications ranging from the capture of energy by photosynthetic

protein complexes, to page ranking algorithms used by search engines. This package was ported to and expanded in the *Julia* programming language by [Glos et al. \(2018\)](#).

In order to truly harness the power of quantum computing, however, one must be able to perform these algorithms on quantum hardware. For this purpose, various implementations of quantum walks on quantum circuits have been purposed. [Douglas \(2009\)](#) pioneered this approach by developing efficient quantum circuits for discrete-time quantum walks on highly symmetric graphs, whose resources scale logarithmically with the size of the state space. [Shakeel \(2020\)](#) presented a new approach for building circuits for the discrete model, reducing resource requirement by using the quantum Fourier transform. For the continuous-time quantum walk, work by [Qiang et al. \(2016\)](#) presents efficient quantum circuits for the circulant graph class, and also an experimental implementation on a photonic quantum processor. In the same year, [Loke and Wang \(2017a\)](#) showed how to build continuous-time quantum walk circuits for composite graphs, namely commuting graphs and Cartesian product of graphs. Considering the Szegedy quantum walk, [Chiang et al. \(2009\)](#) proposed an efficient method of creating quantum circuits for this model. In their work, they showed how to derive a quantum version of the arbitrary sparse classical random walk by approximating a *quantum update rule* with circuit complexity scaling linearly with the degree of sparseness of the structure. [Loke and Wang \(2017b\)](#) developed this method by showing that an efficient circuit for the Szegedy quantum walk can be constructed even if the structures are not sparse, given they possess translational symmetry in the columns of the transitional matrix. More specifically, they identified that the class of cyclic and bipartite graphs are compatible with this approach. Another interesting result in this paper was the creation of circuits that implement a quantum analogue of Google's *Page Rank* algorithm, in terms of Szegedy walks.

On the experimental side, there have been various implementations of quantum walks on quantum computers. On IBM's hardware, work by [Balu et al. \(2017\)](#) presents an efficient implementation of topological quantum walks where they ran the circuit on a five qubit computer over a 4 vertex lattice. [Georgopoulos and Zuliani \(2019\)](#) implements two instances of the discrete-time quantum walk. The first is based on the work of [Douglas \(2009\)](#) using generalized CNOT gates, and the second uses a rotational approach to the CNOT decomposition, which saves using an extra ancilla qubit register. They noted that IBM's simulator backend corresponded to the theoretical predictions, however the circuit for over three qubits was too much for the quantum hardware at that time. The paper presented by [Shakeel \(2020\)](#) also uses IBM's hardware to perform their formulation of the discrete-time quantum walk. For the staggered quantum walk model, work by [Acasiete et al. \(2020\)](#) obtains meaningful results when using the quantum computers to study the dynamics of this model on various graphs with 16 elements, requiring 4 qubits. They also modify these circuits to accommodate an oracle, showing that a spatial search algorithm could be

performed on IBM's quantum computers for a search space of size 8, and with a bit of noise but still satisfactory for size 16.

1.4 OBJECTIVES, CONTRIBUTIONS AND STRUCTURE

The motivation behind the contents in this dissertation is to create an expanded overview on the topic of quantum random walks. To better contextualize the rest of this thesis, appendix A.1 presents the basic concepts and mathematical tools needed to study quantum walks.

Chapter 2 consists of the study of three major quantum random walk models, more specifically the discrete-time coined quantum walk, the continuous-time quantum walk and the staggered quantum walk. For each of these models, this work presents the theoretical framework as well as the corresponding Python implementations. In these simulations, the dynamics of the walks are analyzed by changing various parameters, plotting the resulting probability distributions and seeing how these parameters alter the shape, propagation and other features of the quantum random walks.

Chapter 3 follows this approach, but now the structure where these walks take place is a complete graph and the goal is to find a marked element. For this purpose, the section about Grover's algorithm is used to introduce the notion of quantum searching problems. The following sections show how to change the various models of quantum walks to accommodate an oracle, thus performing an element search in time similar to Grover's algorithm.

Finally, chapter 4 is dedicated to constructing circuits for the models previously defined, using IBM's software *Qiskit* and their hardware. The first three sections are used to create circuits for the dynamics of the walks. The biggest contribution is the circulant graph approach to build diagonal operators for the continuous-time quantum walk, which can be easily translated to Qiskit circuits. Although work by [Qiang et al. \(2016\)](#) pioneered this approach, the work presented in this thesis aims to give a clear description on how to build these circuits in Qiskit and an original analysis on how the approximate quantum Fourier transform affects the accuracy of the results and the number of operations needed to perform the quantum walk. The last section shows how to introduce an oracle to the various circuits in order to perform a searching problem. For the continuous-time case, circulant graphs are again used in an original implementation of the searching problem making use of diagonal operators and the Suzuki-Trotter expansion.

The work reported in this dissertation is partially documented in an accepted paper, and a poster submitted in June 2021:

- Jaime Santos, Bruno Chagas, Rodrigo Chaves. Quantum Walks on a Superconducting Quantum computer. (**accepted** in SBRC 2021 - WQuantum / Comunicação e Computação Quântica)
- Jaime Santos, Bruno Chagas. Implementing Grover's algorithm on a Superconducting Quantum Computer. (**accepted** to the 2nd European Quantum Technologies Virtual Conference)

A third publication

- Jaime Santos, Bruno Chagas. Searching with Continuous-Time Quantum Walks. (in preparation)

is being prepared at the moment of writing.

QUANTUM WALKS

The structure of this chapter is as follows. The first section presents a brief introduction to random walks by reviewing the classical case. The following sections are dedicated to the study of several quantum random walk models and their advantages. This analysis is done by firstly describing the theoretical framework for these walks, and then simulating them in Python, with code that can be found on *Github* ¹.

Section 2.2 introduces the quantum case of random walks by analyzing the dynamics of the coined model, making use of Python's plot capabilities in order to visualize the probability distributions associated with this algorithm. The quantum walk is generally said to be *quadratically* faster than the classical one, which is reflected on the behavior of the standard deviation associated with the probability distribution, and in this section a brief comparison of this metric is also presented. Section 2.3 is dedicated to the study of another instance of a discrete quantum walk, but where a coin is not needed. Instead, *tessellations* are used to construct the Hamiltonians of this algorithm, hence the name *staggered*, effectively reducing the associated Hilbert space. Here, plots are used to study the propagation of the walk, and the effects of altering available the parameters will also be analyzed. Lastly, section 2.4 presents the continuous-time model of the quantum walk. Following the previous sections, the probability distributions will be plotted for the different parameters that can be altered. Finally, this chapter is closed with some final thoughts and remarks.

2.1 CLASSICAL RANDOM WALK

The term *random walk*, firstly introduced by [Pearson \(1905\)](#), is classically defined as a stochastic process that models the path a walker would take through a mathematical space, where each step made by the walker is random. This can be used to model systems such as a molecule displaying Brownian motion in a fluid, or even fluctuating stock prices as in [Sottinen \(2001\)](#).

The simplest instance of this walk is on an infinite discretely numbered line, whose mathematical space is composed of integer numbers. Here, the walker can only advance

¹ <https://github.com/JaimePSantos/QWSimulations>

with equal probability in one of two directions, depending on the outcome of a random event such as tossing a coin. Starting from position $x = 0$, the walker moves to $x = +1$ or $x = -1$ with $\frac{1}{2}$ probability after the first toss. On the second toss, the walker could be on $x = \pm 2$ with $\frac{1}{4}$ probability each, and on $x = 0$ with $\frac{1}{2}$. Continuing this trend will result in a normal probability distribution around the origin, as seen in the Python plot of figure 1.

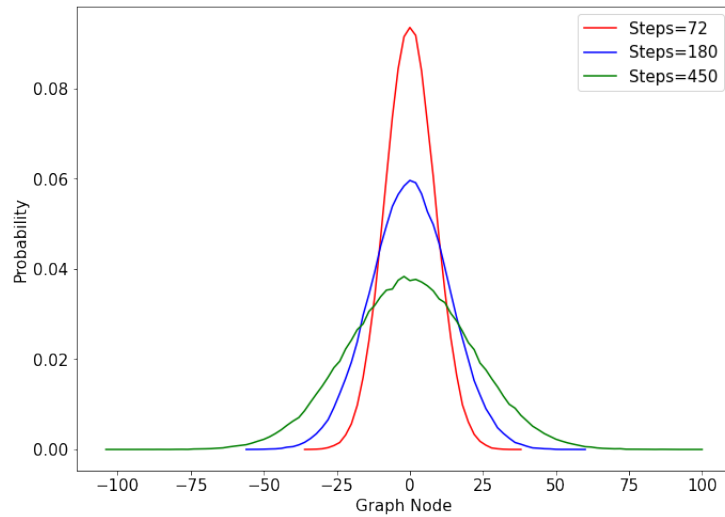


Figure 1: Probability distribution for the classical random walk on a line, after 72, 180 and 450 steps, running 300000 experiments for each number of steps, with starting position on vertex 0.

The number of iterations directly affects how far the walker can reach. As the number of steps increases, the height of each curve at the starting position decreases and the width of the curve increases. This relationship can be captured by the *position standard deviation*, and Pearson (1905) shows that the standard deviation is

$$\sigma(t) \sim \sqrt{t}. \quad (1)$$

In other words, equation (1) represents the rate at which a walker moves away from the origin.

Note that this algorithm can be abstracted to graphs of higher dimensions. For example, in a two dimensional lattice, a walker would be transversing a plane with integer coordinates, choosing one of four directions at every intersection. Notably, Pólya (1921) proved that a walker in a two dimensional lattice will almost surely return to the origin at some point. However, the probability of returning to the origin decreases as the number of dimensions increases, as shown by Montroll (1956) and Finch (2003). It is worth noting that a random walk, over a graph whose nodes are weighed and directed, is analogous to a *discrete-time Markov chain*².

² A Markov chain can be described as a sequence of stochastic events where the the probability of each event depends only on the state of the previous event.

2.2 COINED QUANTUM WALK

In the quantum case, the walker is a system whose position, on an infinite discretely numbered line, is described by a vector $|x\rangle$ in Hilbert space. The next position of the system will depend, in part, of a unitary operator, which can be viewed as a quantum coin. The analogy is, if the coin is tossed and rolls "heads", for example, the system transitions to position $|x + 1\rangle$, otherwise it advances to $|x - 1\rangle$. From a physical perspective, this coin can be the spin of an electron or the chirality of a particle, for example, and the outcome of measuring these properties decides whether the walker moves left or right. The coin is a unitary operator defined as

$$\begin{cases} C|0\rangle = a|0\rangle + b|1\rangle; \\ C|1\rangle = c|0\rangle + d|1\rangle, \end{cases} \quad (2)$$

where a, b, c and d are the complex amplitudes associated with each outcome of the coin toss. One of the most commonly used coins is the unbiased coin, also known as the Hadamard operator

$$H = \begin{pmatrix} a & c \\ b & d \end{pmatrix} = \frac{1}{\sqrt{2}} \begin{pmatrix} 1 & 1 \\ 1 & -1 \end{pmatrix}, \quad (3)$$

which will be the one used in this example.

The Hilbert space of the system is $\mathcal{H} = \mathcal{H}_C \otimes \mathcal{H}_P$, where \mathcal{H}_C is the two-dimensional Hilbert space associated with the coin and \mathcal{H}_P is the Hilbert space of the walker.

The transition from $|x\rangle$ to either $|x + 1\rangle$ or $|x - 1\rangle$ must be described by a unitary operator, the *shift operator*

$$\begin{cases} S|0\rangle|x\rangle = |0\rangle|x + 1\rangle \\ S|1\rangle|x\rangle = |1\rangle|x - 1\rangle, \end{cases} \quad (4)$$

that can also be described by

$$S = |0\rangle\langle 0| \otimes \sum_{x=-\infty}^{x=\infty} |x + 1\rangle\langle x| + |1\rangle\langle 1| \otimes \sum_{x=-\infty}^{x=\infty} |x - 1\rangle\langle x|. \quad (5)$$

It follows that the operator that describes the dynamics of the quantum walk will be given by

$$U = S(C \otimes I) = S(H \otimes I). \quad (6)$$

Consider a quantum system located at $|x = 0\rangle$ with coin state $|0\rangle$, for $t = 0$. Its state will be described by

$$|\psi(0)\rangle = |0\rangle|x = 0\rangle. \quad (7)$$

After t steps

$$|\psi(t)\rangle = U^t |\psi(0)\rangle, \quad (8)$$

more explicitly

$$|\psi(0)\rangle \xrightarrow{U} |\psi(1)\rangle \xrightarrow{U} |\psi(2)\rangle \xrightarrow{U} (\dots) \xrightarrow{U} |\psi(t)\rangle. \quad (9)$$

In summary, the coined quantum walk algorithm consists of applying the coin operator followed by the shift operator a certain number of times. Iterating this twice, evolves the system to the following states

$$|\psi(1)\rangle = \frac{|0\rangle |x = -1\rangle + |1\rangle |x = 1\rangle}{\sqrt{2}} \quad (10)$$

$$|\psi(2)\rangle = \frac{|0\rangle |x = -2\rangle + |1\rangle |x = 0\rangle + |0\rangle |x = 0\rangle - |1\rangle |x = 2\rangle}{2} \quad (11)$$

If one were to measure the system after the first application of U , it would be expected to see the walker at $x = 1$ with probability $P(x) = \frac{1}{2}$, and at $x = -1$ with $P(x) = \frac{1}{2}$. Measure the system t times, after each application of U , and the result is a binomial probability distribution similar to the one in figure 1. The conclusion is that repetitive measurement of a coined quantum walk system reduces to the classical case, which means that any desired quantum behavior is lost.

It is possible, however, to make use of the quantum correlations between different positions to generate constructive or destructive interference, by applying the Hadamard and shift operators successively without intermediary measurements. The consequences of interference between states become very apparent after only 3 iterations

$$|\psi(3)\rangle = \frac{|1\rangle |x = -3\rangle - |0\rangle |x = -1\rangle + 2(|0\rangle + |1\rangle) |x = 1\rangle + |0\rangle |x = 3\rangle}{2\sqrt{2}}. \quad (12)$$

Even though an unbiased coin was used, this state is not symmetric around the origin and the probability distributions will not be centered in the origin. Moreover, Childs et al. (2002) shows that the standard deviation will be

$$\sigma(t) \approx 0.54t. \quad (13)$$

This means that the standard deviation for the coined quantum walk grows linearly in time, unlike the classical case which grows with \sqrt{t} , as seen in equation (1). The implication is that the quantum walk displays *ballistic* behavior, as is reviewed in Venegas-Andraca (2012). This behavior is usually defined in the context of a moving free particle with unit velocity in a single direction, which is expected to be found at $x = t$ after t steps. The velocity of a walker in a Hadamard quantum walk is approximately half of the free particle example, which is still a quadratic improvement over the classical random walk. Figure 2 shows the comparison between the evolution of the classical and the quantum standard deviation.

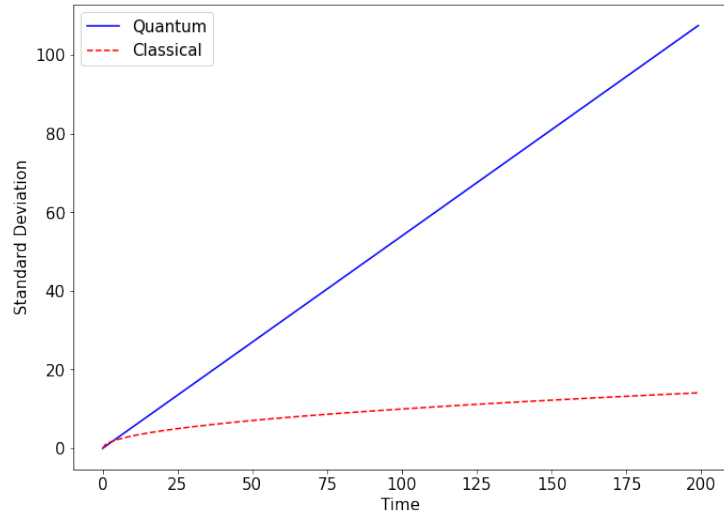


Figure 2: Standard deviation after 200 steps for the quantum walk in blue, and the classical random walk in red.

This quadratic gain implies exponentially faster hitting times in certain graphs, as shown by [Childs et al. \(2002\)](#), meaning improvements to problems that require transversing graphs. [Ambainis \(2007\)](#) also shows advantages of the coined quantum walk model in element distinctness problems, and [Childs and Goldstone \(2004\)](#) show advantages in spatial search problems, which will be studied in a later chapter.

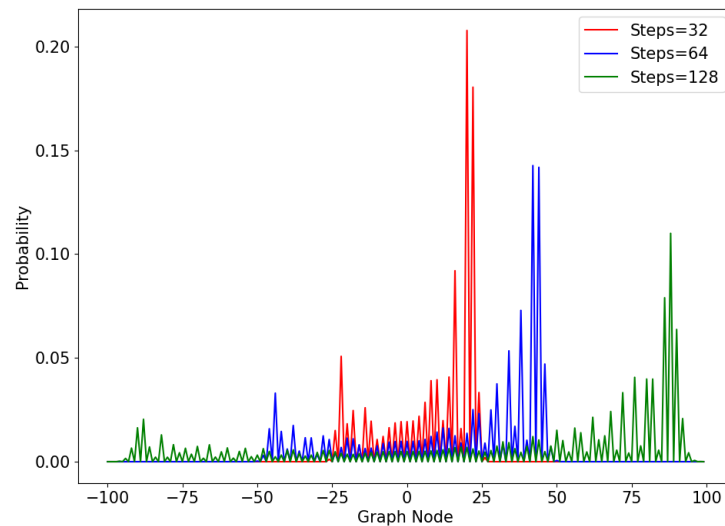


Figure 3: Probability distribution for the coined quantum walk on a line, after 32, 64 and 128 steps, with initial condition $|\psi(0)\rangle = |0\rangle |x=0\rangle$ and the Hadamard coin.

In order to study this distribution, a simulation of the coined quantum walk was coded in *Python*. Figure 3 is the result of using the Hadamard coin and the initial condition in equation 7, for varying numbers of steps. Analyzing the plot, it is noticeable that the distributions are asymmetric. The probability of finding the walker on the right-hand side is much larger than on the left, with a peak around $x \approx \frac{t}{\sqrt{2}}$. Regardless of number of steps, this peak is always present (albeit in varying positions), which is to say that the walker can always be found moving in a uniform fashion away from the origin, consistent with ballistic behaviour.

Another interesting case study is to find if this behavior is preserved for a symmetric distribution around the origin. For this purpose, one must first understand where the asymmetry comes from. The Hadamard operator flips the sign of state $|1\rangle$, hence more

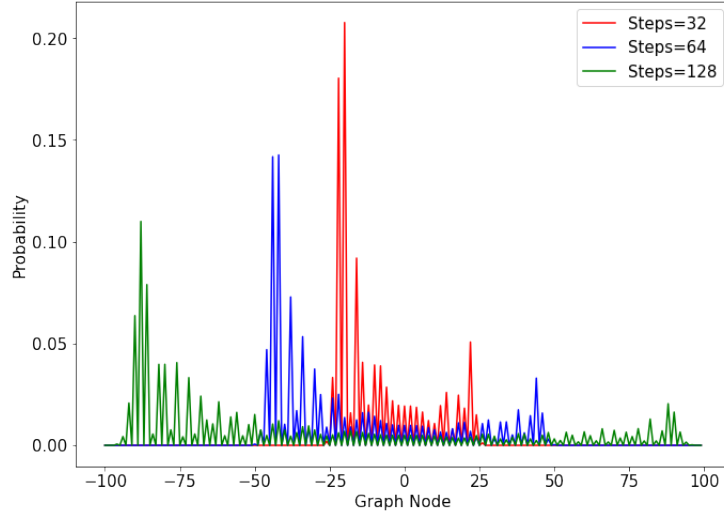


Figure 4: Probability distribution for the coined quantum walk on a line, after 32, 64 and 128 steps, with initial condition $|\psi(0)\rangle = |1\rangle |x = 0\rangle$ and the Hadamard coin.

terms are canceled when the coin state is $|1\rangle$. Since $|0\rangle$ was defined to induce movement to the right, the result is as shown in figure 3. Following this logic, it would be expected that an initial condition

$$|\psi(0)\rangle = |1\rangle |x = 0\rangle, \tag{14}$$

would result in more cancellations when the coin state is $|0\rangle$, thus the walker would be more likely found in the left-hand side of the graph. This is indeed what happens, as figure 4 is a mirror image of figure 3. The walker still moves away from the origin with ballistic behavior, but in the opposite direction. The peaks behave in a similar fashion, being found instead at $x \approx -\frac{t}{\sqrt{2}}$.

In order to obtain a symmetrical distribution, one must superpose the state in equation (7) with the state in equation 14. However, in order to not cancel terms before the calculation of the probability distribution, one must multiply state $|1\rangle$ with the imaginary unit, i

$$|\psi(0)\rangle = \frac{|0\rangle + i|1\rangle}{\sqrt{2}} |x = 0\rangle. \quad (15)$$

The entries of the Hadamard operator are real numbers, therefore terms with the imaginary

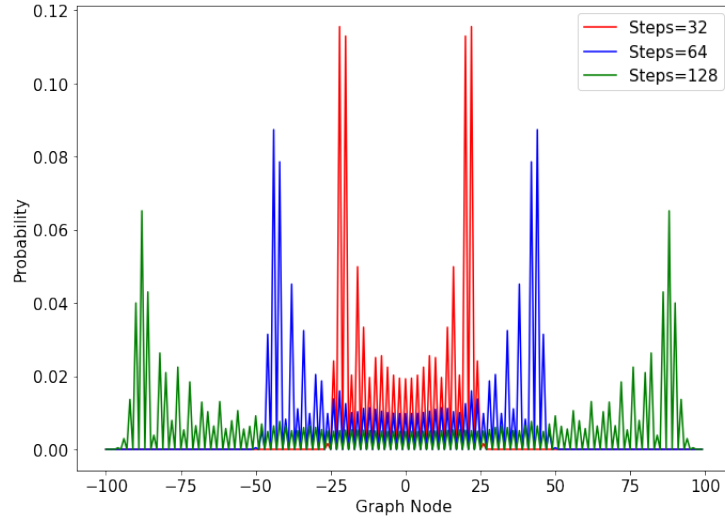


Figure 5: Probability distribution for the coined quantum walk on a line, after 32, 64 and 128 steps, with initial condition $|\psi(0)\rangle = \frac{|0\rangle + i|1\rangle}{\sqrt{2}} |x = 0\rangle$ and the Hadamard coin.

unit will not cancel out with terms without it, thus the walk can proceed to both left and right, as shown in figure 5. Note that using another coefficient for i will result in nontrivial behaviour. The probability distribution is now symmetric and it is spread over the range $[-\frac{t}{\sqrt{2}}, \frac{t}{\sqrt{2}}]$ with peaks around $x \approx \pm \frac{t}{\sqrt{2}}$. This means that if the position of the walker was measured at the end, it would be equally probable to find him far away from the origin, either in the left side or the right side of the graph, which is not possible in a classical random walk.

All of the previous examples are in sharp contrast with the classical random walk distribution in figure 1. There, the maximum probability is reached at $x = 0$ since there are approximately equal steps in both directions. Furthermore, the further the vertex is away from the origin, the less likely the walker is to be found there. However, in the quantum case, the walker is more likely to be found away from the origin as the number of steps increases. More specifically, the walk spreads quadratically faster than the classical counterpart.

This is but one model of a quantum random walk. As it will be seen in further sections, there are other approaches to creating both discrete and continuous-time quantum walk models that do not use a coin.

2.3 STAGGERED QUANTUM WALK

The staggered quantum walk (SQW) model aims to spread a transition probability to neighboring vertices with discrete time steps. The notion of adjacency comes from cliques³, and the initial stage of this walk consists of partitioning the graph into several different cliques. This is known as the *tessellation* process. An element of a tessellation \mathcal{T} is called a polygon, and it is only valid if all of its vertices belong to the clique in \mathcal{T} . The set of polygons of each tessellation must cover all vertices of the graph, and the set of tessellations $\{\mathcal{T}_1, \mathcal{T}_2, \dots, \mathcal{T}_k\}$ must cover all the edges.

These definitions allow the construction of operators H_1, H_2, \dots, H_k to propagate the probability amplitude locally, in each polygon. The state associated to each polygon is

$$|u_j^k\rangle = \frac{1}{\sqrt{|\alpha_j^k|}} \sum_{l \in \alpha_j^k} |l\rangle, \quad (16)$$

where α_j^k is the j^{th} polygon in the k^{th} tessellation.

The unitary, local and Hermitian operator H_k , associated to each tessellation is defined in Portugal et al. (2017) as

$$H_k = 2 \sum_{j=1}^p |u_j^k\rangle \langle u_j^k| - I. \quad (17)$$

Solving the time-independent Schrodinger equation for this Hamiltonian gives the evolution operator

$$U = e^{i\theta_k H_k} \dots e^{i\theta_2 H_2} e^{i\theta_1 H_1}, \quad (18)$$

where

$$e^{i\theta_k H_k} = \cos(\theta_k) I + i \sin(\theta_k) H_k, \quad (19)$$

since $H_k^2 = I$, meaning that the Hamiltonian is a reflection operator that, when expanded in a Taylor series, generates a local operator.

The simplest use case of this quantum walk model is the one-dimensional lattice, where the minimum tessellations are

$$\mathcal{T}_\alpha = \{\{2x, 2x + 1\} : x \in \mathbb{Z}\}, \quad (20)$$

$$\mathcal{T}_\beta = \{\{2x + 1, 2x + 2\} : x \in \mathbb{Z}\}. \quad (21)$$

Each element of the tessellation has a corresponding state, as can be seen in figure 6, and

³ A clique is defined as the subset of vertices of an undirected graph such that every two distinct vertices in each clique are adjacent.

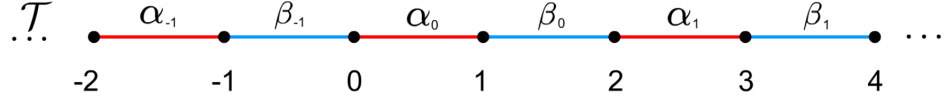


Figure 6: Tessellation of a line graph.

the uniform superposition of these states is

$$|\alpha_x\rangle = \frac{|2x\rangle + |2x+1\rangle}{\sqrt{2}}, \quad (22)$$

$$|\beta_x\rangle = \frac{|2x+1\rangle + |2x+2\rangle}{\sqrt{2}}. \quad (23)$$

One can now define Hamiltonians H_α and H_β as

$$H_\alpha = 2 \sum_{x=-\infty}^{+\infty} |\alpha_x\rangle \langle \alpha_x| - I, \quad (24)$$

$$H_\beta = 2 \sum_{x=-\infty}^{+\infty} |\beta_x\rangle \langle \beta_x| - I. \quad (25)$$

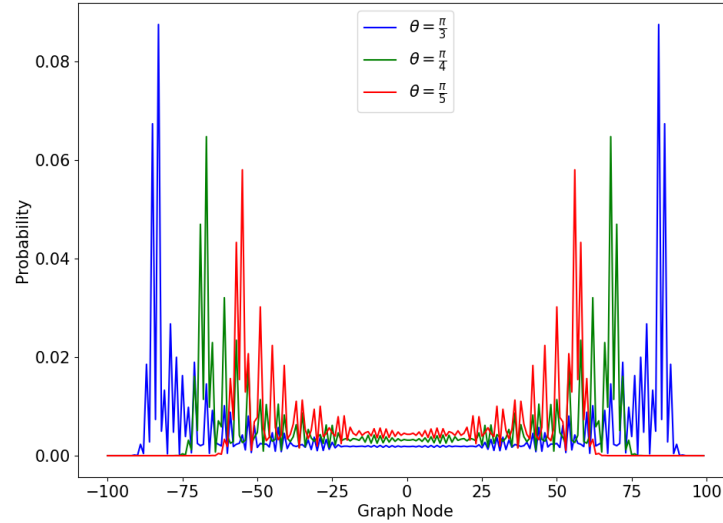


Figure 7: Probability distribution for the staggered quantum walk on a line after 50 steps, with initial condition $|\psi(0)\rangle = \frac{|0\rangle + |1\rangle}{\sqrt{2}}$, for multiple values of θ .

The Hamiltonian evolution operator reduces to

$$U = e^{i\theta H_\beta} e^{i\theta H_\alpha}, \quad (26)$$

and applying it to an initial condition $|\psi(0)\rangle$ results in the time evolution operator

$$U |\psi(t)\rangle = U^t |\psi(0)\rangle. \quad (27)$$

Having defined the time evolution operator, the walk is ready to be coded with a certain initial condition and θ value, to better understand how the probability distribution spreads through time. For the first case study, the initial condition will be a uniform superposition of states $|0\rangle$ and $|1\rangle$ and the value of θ will be varied in order to understand how this parameter impacts the walk, as seen in figure 7. The overall structure of the probability distribution is very similar for different values of θ , the difference being that the walker is more likely to be found further away from the origin as the angle increases.

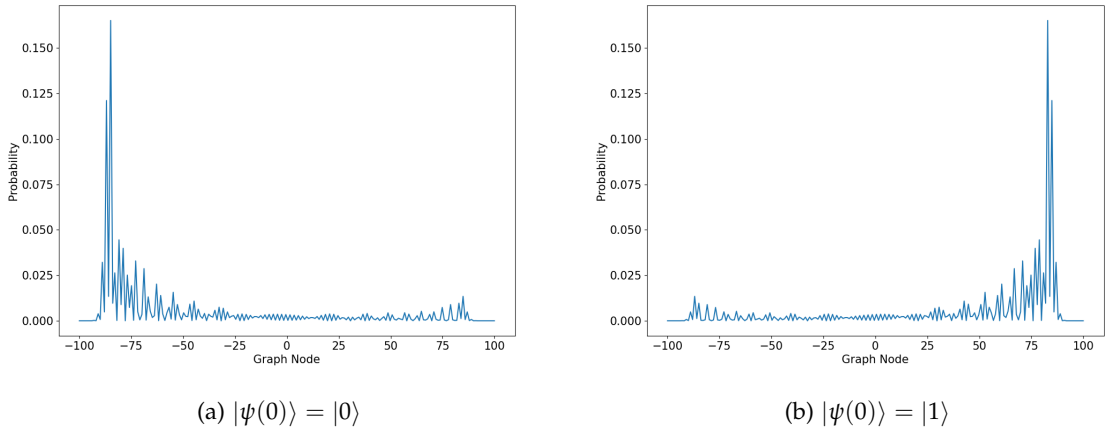


Figure 8: Probability distributions for the staggered quantum walk on a line after 50 steps, for different initial conditions.

Another interesting case study is to see how the initial condition affects the dynamics of the system, and figure 8 shows the results of plotting the quantum walk for initial conditions $|\psi(0)\rangle = |0\rangle$ and $|\psi(0)\rangle = |1\rangle$. Similarly to the coined case, each initial condition results in asymmetric probability distributions, $|\psi(0)\rangle = |0\rangle$ leads to a peak in the left-hand side, while condition $|\psi(0)\rangle = |1\rangle$ results in a peak in the right-hand side. As shown in figure 7, the uniform superposition of both these conditions results in a symmetric probability distribution.

So far, only discrete-time quantum walks have been shown. The next section presents the continuous-time quantum walk model, where time is not discretized and whose Hilbert space is the space of the walker.

2.4 CONTINUOUS-TIME QUANTUM WALK

The continuous-time random walk model on a graph is a Markov process where transitions have a fixed probability per unit time, γ , of moving to adjacent vertices, firstly introduced by [Montroll and Weiss \(1997\)](#). Consider a graph G with N vertices and no self-loops, this walk can be defined by the linear differential equation that describes the probability of jumping to a connected vertex in any given time

$$\frac{dp_i(t)}{dt} = \gamma \sum_j L_{ij} p_j(t), \quad (28)$$

where L is the Laplacian defined as $L = A - D$, and $p_j(t)$ is the time dependent probability associated with each vertex transition. A is the adjacency matrix that represents each vertex connection, given by

$$A_{ij} = \begin{cases} 1, & \text{if } (i, j) \in G \\ 0, & \text{otherwise,} \end{cases} \quad (29)$$

and D is the diagonal matrix $D_{jj} = \text{deg}(j)$ corresponding to the degree⁴ of vertex j .

In the continuous-time quantum walk model (CTQW), the vertices are quantum states that form the basis for the Hilbert space. The continuous-time quantum walk model will also be described by a differential equation, the Schrödinger equation

$$i\hbar \frac{d|\psi(t)\rangle}{dt} = H|\psi(t)\rangle, \quad (30)$$

where $H = -\gamma L$ is the Hamiltonian of the system. More explicitly,

$$H_{ij} = \begin{cases} \text{deg}(j)\gamma, & \text{if } i = j; \\ -\gamma, & \text{if } i \neq j \text{ and adjacent;} \\ 0, & \text{if } i \neq j \text{ and not adjacent.} \end{cases} \quad (31)$$

A general state of a system $|\psi(t)\rangle$ can be written as a function of its complex amplitudes

$$q_i = \langle i|\psi(t)\rangle, \quad (32)$$

which means equation (30) can be rewritten as

$$i\hbar \frac{dq_i(t)}{dt} = \sum_j H_{ij} q_j(t). \quad (33)$$

⁴ The degree of a vertex refers to the number of edges that it is connected to.

Comparing equations (33) and (28), the Laplacian is replaced by the Hamiltonian, and the probabilities by amplitudes. One of the main differences is the complex phase i , which will result in a very different behavior. Setting $\hbar = 1$ and solving the differential equation results in the evolution operator of this walk

$$U(t) = e^{-iHt} = e^{i(\gamma L)t} = e^{i\gamma(A-D)t}, \quad (34)$$

In the regular graph case, where D is simply the degree of the graph multiplied by the identity matrix, A and D will commute, meaning that the evolution operator can be written in terms of the adjacency matrix

$$U(t) = e^{i\gamma At - i\gamma Dt} = e^{i\gamma At} e^{-i\gamma Dt} = \phi(t) e^{i\gamma At}, \quad (35)$$

since the degree matrix becomes a global phase. Applying this operator to an initial condition $\psi(0)$, will give the state of the system at a time t

$$|\psi(t)\rangle = U(t) |\psi(0)\rangle. \quad (36)$$

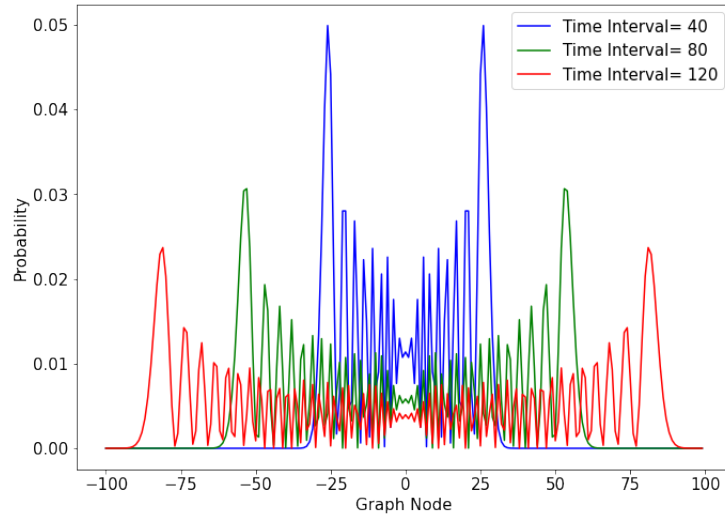


Figure 9: Probability distribution for the continuous-time quantum walk on a line, at $t = 40, 80$ and 120 , with initial condition $|\psi(0)\rangle = |0\rangle$ and $\gamma = \frac{1}{2\sqrt{2}}$.

Considering a uni-dimensional quantum system, each vertex will have at most 2 other neighboring vertices, reducing equation (31) to

$$H_{ij} = \begin{cases} 2\gamma, & \text{if } i = j; \\ -\gamma, & \text{if } i \neq j \text{ and adjacent;} \\ 0, & \text{if } i \neq j \text{ and not adjacent.} \end{cases} \quad (37)$$

For a more detailed visualization, this quantum walk model was coded in Python and figure 9 was obtained setting the transition rate to $\gamma = \frac{1}{2\sqrt{2}}$ and the initial condition to $|\psi(0)\rangle = |0\rangle$. A brief look at figure 9 reveals several similarities to previous models. The property of having two peaks away from the origin and low probability near the origin is present across all the quantum walks. However, in the continuous case, a symmetric initial condition is not needed. In the staggered quantum walk model, the propagation of the walk could be altered by changing the values of θ , whereas in this case different values of γ and time will influence the probability distribution.

Altering the initial condition will also differ in the continuous-time example. For example, setting the initial condition to the balanced superposition of states $|0\rangle$ and $|1\rangle$ has no effect on the overall pattern of the probability distribution as seen in figure 10. Both peaks are still present and at the same distance from the origin, with intermediate amplitudes being attenuated relative to figure 9. This behavior is in contrast with the previous discrete-time cases, where a change in the initial condition would dictate the number of peaks and where they would appear. Figure 10 also shows the influence of the transition rate γ . As would

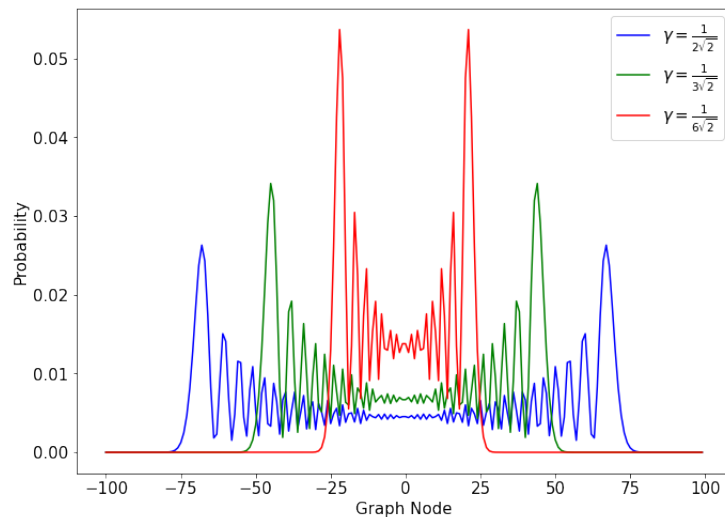


Figure 10: Probability distribution for the continuous-time quantum walk on a line, at $t = 100$, with initial condition $|\psi(0)\rangle = \frac{|0\rangle + |1\rangle}{\sqrt{2}}$, for multiple values of γ .

be expected from equation (35), the effects are very similar to altering time, since both parameters are multiplying in the exponential.

In conclusion, the purpose of this chapter was to present an overview of several different models of a quantum walk. The probability distributions are very distinct from the classical case, but relatively similar to each other. The bigger differences between the models come from the size of the associated Hilbert space. The staggered and continuous-time quantum walks have Hilbert spaces equal to the space of the walker, whereas the coined quantum walk also requires a space for the coin. It might seem unimportant now, but it will play a

major role when these models are translated into circuits, since the size of the Hilbert space will have a direct relation with the number of qubits required to perform the walk, which is a scarce resource for *Noisy intermediate-scale quantum* (NISQ) computers. Considering the case of the coined quantum walk on a simple line graph, only one extra qubit will be needed. However, as will be seen in the next chapter, the search problem is optimal when performed over a complete graph which, in the coined case, will double the number of required qubits.

SEARCHING PROBLEMS

This chapter studies the search problem using quantum walks. Section 3.1 introduces the basics of a search problem by presenting the theoretical framework of Grover's algorithm, followed by a complexity analysis, together with Python plots for a better illustration. Different numbers of marked elements will be shown and, by the end of the section, it should be clear that Grover's algorithm is optimal for searching, as shown by Zalka (1999).

Subsequent sections are dedicated for the quantum walk instance of this problem. In section 3.2, the coined quantum walk is defined for the search problem, which implies the introduction of an oracle. Here, instead of a line, a complete graph is used, which will increase the space of the search to $2N$, due to the connected nature of this graph and the need of a coin. Section 3.3 presents the staggered quantum walk version of the search problem. Again, the notion of cliques and tessellations is used instead of a coin, and the complete graph is again considered. The oracle is again defined for this walk, which makes it quite similar to Grover's algorithm. However, since it is possible to alter the parameter θ and the structure over which the search is performed, this algorithm is known to be more general than Grover's. Like the coined quantum walk, the staggered model is discrete in time but, since a coin is not used, the space associated with it scales only with the size of the graph, meaning its implementation on a NISQ computer will be more feasible. Finally, section 3.4 closes this chapter with the search instance of the continuous-time quantum walk. Similarly to the staggered quantum walk, both the structure where the search is performed and parameter γ can be controlled. However, because time is not discrete in this instance, the probability distribution associated with this walk will be slightly different, and it will later be seen that this results in a circuit that does not scale up with time.

3.1 GROVER'S ALGORITHM

Searching through an unstructured database is a task classically achieved by exhaustively evaluating every element in the database. Assume there exists a black box (oracle) that can be asked to find out if two elements are equal. Since we're looking for a specific element in

a database of size N , we'd have to query the oracle on average $\frac{N}{2}$ times or, in the worst case, N times.

Grover's algorithm, presented in Grover (1996), comes as a quantum alternative to this type of problems, taking advantage of superposition by increasing desirable states' amplitudes through a process called *amplitude amplification*. This method has a quadratic gain over the classical counterpart, shown in Boyer et al. (1998), being able to find a target element in expected time $\mathcal{O}(\sqrt{N})$.

The inner workings of the black box will now be expanded upon. Instead of directly evaluating the elements, the searching indices will be considered, and the number of elements defined as $N = 2^n$, n being a positive integer. The next step is to define a function $f : \{0, 1, \dots, N - 1\}$ that returns 1 when evaluating the desired (marked) element, and 0 otherwise. Since this function is to be applied to a quantum system, a unitary operator can be built such as

$$\mathcal{O} |x\rangle |i\rangle = |x\rangle |i \oplus f(x)\rangle. \tag{38}$$

where $|x\rangle$ is the index register, \oplus is the binary sum operation and $|i\rangle$ is a qubit that is flipped if $f(x) = 1$.

The action of the oracle on state $|0\rangle$ will be

$$\mathcal{O} |x\rangle |0\rangle = \begin{cases} |x_0\rangle |1\rangle, & \text{if } x = x_0 \\ |x\rangle |0\rangle, & \text{otherwise.} \end{cases} \tag{39}$$

where x_0 is the marked element. More generically, \mathcal{O} can be written as

$$\mathcal{O} |x\rangle = (-1)^{f(x)} |x\rangle. \tag{40}$$

This offers a bit of insight into the oracle: it *marks* the solutions to the search problem by applying a phase shift to the solutions. The question now is, what is the procedure that determines a solution x_0 using \mathcal{O} the minimum number of times? The answer lies in the amplitude amplification section of Grover's search, starting with the creation of a uniform superposition

$$|\psi_0\rangle = H^{\otimes n} |0\rangle = \frac{1}{\sqrt{N}} \sum_{x=0}^{N-1} |x\rangle, \tag{41}$$

where $H^{\otimes n}$ is the *Hadamard* operator applied to an arbitrary number of qubits.

If one were to measure $|x\rangle$ at this point, the superposition would collapse to any of the base states with the same probability $\frac{1}{N} = \frac{1}{2^n}$, which means that on average, we'd need to try $N = 2^n$ times to guess the correct item. This is where amplitude amplification comes into effect, by means of a second unitary operator

$$\mathcal{D} = (2 |\psi_0\rangle \langle \psi_0| - I) = H^{\otimes n} (2 |0\rangle \langle 0| - I) H^{\otimes n}. \tag{42}$$

This operator applies a conditional phase shift, with every computational basis state except $|0\rangle$ receiving a phase shift. This can also be described as the *inversion about the mean*, for a state of arbitrary amplitudes

$$|\phi\rangle = \sum_{k=0}^{N-1} \alpha_k |k\rangle, \quad (43)$$

the action of \mathcal{D} on state ϕ will be

$$\mathcal{D}|\phi\rangle = \sum_{k=0}^{N-1} (-\alpha_k + 2\langle\alpha\rangle) |k\rangle, \quad (44)$$

where $\langle\alpha\rangle$ is the average of α_k

$$\langle\alpha\rangle = \frac{1}{N} \sum_{k=0}^{N-1} \alpha_k |k\rangle. \quad (45)$$

The evolution operator that performs one step of the algorithm is then

$$\mathcal{U} = \mathcal{D}\mathcal{O}, \quad (46)$$

and after t steps the state of the system is

$$|\psi(t)\rangle = \mathcal{U}^t |\psi_0\rangle. \quad (47)$$

3.1.1 One marked element

The optimal number of steps is, as aforementioned, proportional to \sqrt{N} . More precisely, if there's only one solution, maximum probability can be reached in *approximately* $\frac{\pi}{4}\sqrt{N}$ iterations. In order to show that this is the case, an iteration will be formally defined, following the example of [Boyer et al. \(1998\)](#), as the process that transforms the state

$$|\psi(k, l)\rangle = k|i_0\rangle + \sum_{i \neq i_0} l|i\rangle, \quad (48)$$

into state $|\psi(\frac{N-2}{N}k + \frac{2(N-1)}{N}l, \frac{N-2}{N}l - \frac{2}{N}k)\rangle$. Amplitudes l and k are real numbers that satisfy $k^2 + (N-1)l^2 = 1$. Running t iterations over state $|\psi_0\rangle$ will eventually lead to state $|\psi_j\rangle = |\psi(k_j, l_j)\rangle$ after the j^{th} iteration, where $k_0 = l_0 = \frac{1}{\sqrt{N}}$ and

$$\begin{cases} k_{j+1} = \frac{N-2}{N}k_j + \frac{2(N-1)}{N}l_j; \\ l_{j+1} = \frac{N-2}{N}l_j + \frac{2}{N}k_j. \end{cases} \quad (49)$$

After the last iteration, the system will be in state $|\psi_t\rangle$ with a certain amplitude. If that amplitude corresponds to the marked element x_0 , then it is said that the algorithm was successful.

Grover (1996) proves that there exists a value of $t < \sqrt{2N}$, such that the probability of success is at least $\frac{1}{2}$. However the probability of success does not linearly increase with the number of iterations, in fact for $t = \sqrt{2N}$ the system will succeed less than 1 in 10 times. Boyer et al. (1998) argues that an explicit value of t is needed, and this can be achieved by finding a closed form formula for k_j and l_j . The first step is to define an angle θ so that $\sin^2 \theta = \frac{1}{N}$, and equation (49) becomes

$$\begin{cases} k_j = \sin((2j+1)\theta); \\ l_j = \frac{1}{\sqrt{N-1}} \cos((2j+1)\theta). \end{cases} \tag{50}$$

In order to maximize the probability of success, one must find a value of t so that $k_t \approx 1$ and l_t is as close to 0 as possible. The value of k after t iterations will be at its maximum when $\sin((2t+1)\theta) = 1$. Solving the trigonometric equation leads to a value of $t = \frac{\pi-2\theta}{4\theta}$. Conversely, $l_t = 0$ when $\tilde{t} = \frac{\pi-2\theta}{4\theta}$ for an integer number of \tilde{t} . Setting t to $\lfloor \frac{\pi}{4\theta} \rfloor$ will lead to

$$|t - \tilde{t}| \leq \frac{1}{2} \iff |(2t+1)\theta - (2\tilde{t}+1)\theta| \leq \frac{\pi}{2}. \tag{51}$$

By definition, $(2\tilde{t}+1)\theta = \frac{\pi}{2}$ which means that $|\cos((2t+1)\theta)| \leq |\sin \theta|$. The probability of

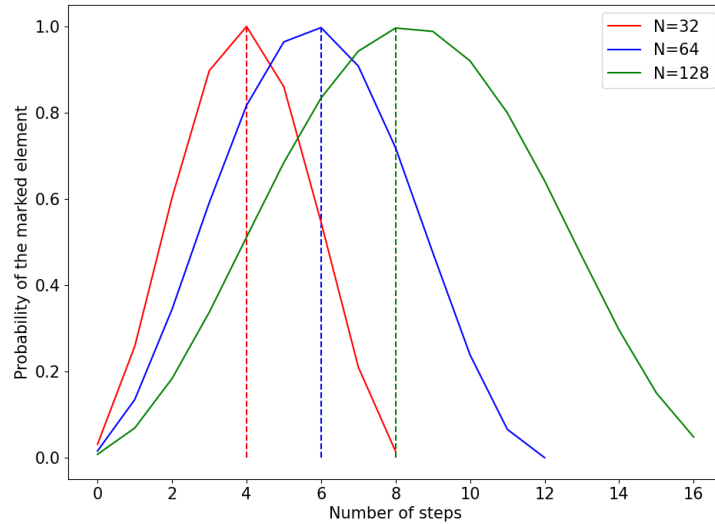


Figure 11: Probability of one marked element in the Grover search, as a function of the number of steps, for $N = 32, 64, 128$ and 256 .

failure after t iterations can then be written as

$$(N-1)l_t^2 = \cos^2((2t+1)\theta) \leq \sin^2\theta = \frac{1}{N}. \quad (52)$$

Failure decreases as the number of elements increases. The run time of the algorithm will be

$$t \leq \frac{\pi}{4\theta} \leq \frac{\pi}{4}\sqrt{N}, \quad (53)$$

since $\theta \geq \sin\theta = \frac{1}{\sqrt{N}}$. This means that, for a large N , the number of iterations that maximizes the probability of success will be very close to $\frac{\pi}{4}\sqrt{N}$.

Figure 11 was obtained by coding the appropriate operators as to simulate the system presented in equation (47). The unitary evolution operator was applied approximately $\frac{\pi}{4}\sqrt{N}$ times and the amplitudes associated with those states were stored as a probability distribution. Filtering the probability of the marked element and plotting it against the number of steps, shows that the maximum is indeed reached after the said number of iterations, and then decreases as more steps are taken, periodically. It also shows that the maximum probability for $N = 32$ is lower than for $N = 128$, which makes sense since the the probability of success is maximized for larger values of N . This is the case because the ideal number of iterations will be $\lfloor \frac{\pi}{4}\sqrt{N} \rfloor$, meaning that the rounding will be proportionally smaller as N increases.

3.1.2 Multiple marked elements

When there's more than one element marked by the oracle, the number of iterations to achieve maximum probability changes. In fact, the latter part of this section will be used to discuss the case where one single iteration of this algorithm is enough to achieve maximum probability.

Firstly, one must define a set A collecting all the marked elements and set B with the remaining ones. The state from equation (48) will become

$$|\psi(k, l)\rangle = \sum_{i \in A} k|i\rangle + \sum_{x \in B} l|x\rangle. \quad (54)$$

Assuming m marked elements, iterating over this state will result in

$$\left| \psi\left(\frac{N-2m}{N}k + \frac{2(N-m)}{N}l, \frac{N-2m}{N}l - \frac{2m}{N}k\right) \right\rangle. \quad (55)$$

Choosing an angle θ such that $\sin^2\theta = \frac{t}{N}$, allows the definition of the amplitudes associated with the states after j iterations

$$\begin{cases} k_j = \frac{1}{\sqrt{m}} \sin((2j+1)\theta); \\ l_j = \frac{1}{\sqrt{N-m}} \cos((2j+1)\theta). \end{cases} \quad (56)$$

Similarly to the one solution case, it can be shown that setting the number of iterations t , to

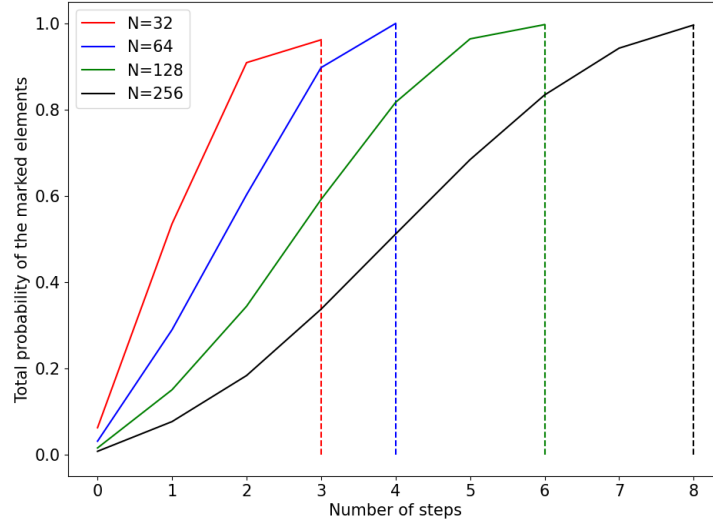


Figure 12: Probability of two marked elements in the Grover search, as a function of the number of steps, for $N = 32, 64, 128$ and 256 .

the nearest lower integer of $\frac{\pi}{4\theta}$ will result in a probability of failure $(N-m)l_t^2 \leq \frac{m}{N}$. Because $\theta \geq \sin\theta = \sqrt{\frac{t}{N}}$, then

$$t \leq \frac{\pi}{4\theta} \leq \frac{\pi}{4} \sqrt{\frac{N}{m}}. \quad (57)$$

From a more practical perspective, if one were to mark two elements of a 64 element set, maximum probability is expected to be reached in approximately 4 steps, since $\lfloor \frac{\pi}{4} \sqrt{\frac{64}{2}} \rfloor = 4$. Likewise, for $N = 256$, the number of iterations is rounded to 8, which is plotted along several other values of N in figure 12. The y-axis is now the sum total probability of the marked elements and the x-axis represents the range of steps that spans from 0 to $\lfloor \frac{\pi}{4} \sqrt{\frac{N}{2}} \rfloor$ for each N . Again, the probability of success approaches 1 as N increases. However, comparing to figure 11, the number of iterations that maximizes probability is lower because of the increased number of marked elements, in agreement with equation (57). Work by Zalka (1999) shows that the time complexity associated to Grover's algorithm is optimal, and that parallelization of quantum searching should not yield better results.

3.1.3 Single-Shot Grover

An interesting case arises when the number of marked elements is set to $m = \frac{N}{4}$, because

$$\sin^2 \theta = \frac{\frac{N}{4}}{N} = \frac{1}{4} \iff \sin \theta = \frac{1}{2} \iff \theta = \frac{\pi}{6}. \quad (58)$$

Note that there are an infinite number of negative and positive solutions, but equation (58)

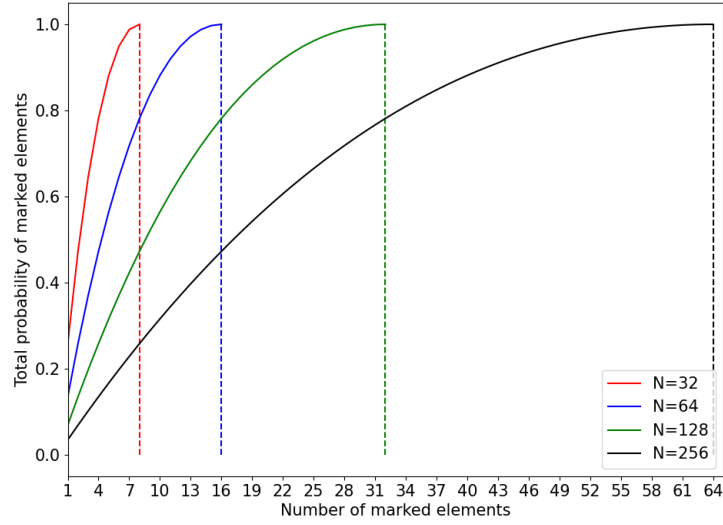


Figure 13: Total probability of marked elements in the Grover search, as a function of the number of marked elements, for 1 step, with $N = 32, 64, 128$ and 256 .

reflects the only relevant one in this context. As a consequence, amplitudes associated with state $|\psi(k_1, l_1)\rangle$ become

$$\begin{cases} k_1 = \frac{1}{\sqrt{m}} \sin((2+1)\theta) = \frac{1}{\sqrt{\frac{N}{4}}} \sin(3\frac{\pi}{6}) = \frac{2}{\sqrt{N}}; \\ l_1 = \frac{1}{\sqrt{N-m}} \cos((2+1)\theta) = \frac{1}{\sqrt{N-\frac{N}{4}}} \cos(3\frac{\pi}{6}) = 0. \end{cases} \quad (59)$$

These results show that the amplitudes associated with the marked states double in relation to $|\psi_0\rangle$ and the remaining states disappear after only one iteration. This behavior can be seen in figure 13, where the total probability of marked elements reaches 1 after a single shot of the Grover procedure, once the number of marked elements is $\frac{1}{4}$ of the total elements.

The following sections will present the search problem in the context of quantum walks. They are generalizations of Grover's algorithm, but implemented in graphs.

3.2 COINED QUANTUM WALK

In classical computation, a *spatial search problem* focuses on finding marked points in a finite region of space. Defining this region with graphs is fairly straightforward, the vertices of the graph are the search space, and the edges define what transitions are possible through the search space. As was previously mentioned in section 3.1, exhaustively searching through an unstructured space, by means of a classical random walk for example, would mean that in the worst case, one would have to take as many steps to find the marked points as there are vertices in the graph. Quantum computing provides a more efficient alternative through Grover's algorithm. Applying some of the underlying ideas to the coined quantum walk not only allows a quantum counterpart to the random walk search, but also further insight into the algorithm itself.

Following Portugal (2018)'s definition, a good first step is to borrow the diffusion from Grover's algorithm and invert the sign of the state corresponding to the marked vertex while leaving unmarked vertices unchanged. This is done through the following operator

$$\mathcal{O} = I - 2 \sum_{x \in M} |x\rangle \langle x|, \quad (60)$$

where M is the set of marked vertices and \mathcal{O} is an analogue to Grover's oracle. For one marked vertex, this oracle can be written as

$$\mathcal{O} = I - 2 |0\rangle \langle 0|. \quad (61)$$

Notice that there is no loss of generality by choosing the marked vertex as 0, since the labeling of the vertices is arbitrary.

The next step is to combine the evolution operator from the coined quantum walk model with the oracle

$$U' = U\mathcal{O}. \quad (62)$$

Similarly to the simple coined case, the walker starts at $|\psi(0)\rangle$ and evolves according to the rules of an unitary operator U , followed by the sign inversion of marked vertices. The walker's state after an arbitrary number of steps will be

$$\psi(t) = (U')^t |\psi(0)\rangle. \quad (63)$$

For a better understanding of the search problem in the coined quantum walk model, consider a graph where all the vertices are connected and each vertex has a loop that allows transitions to itself. The next step is to label the edges using notation $\{(v, v'), v \geq 0 \wedge v' \leq$

$N - 1\}$ where N is the total number of vertices and (v, v') are the position and coin value, respectively. The shift operator, now called the *flip-flop* shift operator, is

$$S |v1\rangle |v2\rangle = |v2\rangle |v1\rangle. \quad (64)$$

The coin operator is defined as

$$C = I_N \otimes G, \quad (65)$$

where

$$G = 2 |s\rangle \langle s| - I \quad (66)$$

is the Grover coin, with $|s\rangle$ being the uniform superposition of the coin states.

Marking an element in a complete graph is done through the following oracle

$$\mathcal{O}' = \mathcal{O} \otimes I = (I_N - 2 |0\rangle \langle 0|) \otimes I_N = I_{N^2} - 2 \sum_v |0\rangle |v\rangle \langle 0| \langle v|, \quad (67)$$

that is seen as an operator that marks all edges leaving 0. Recalling equation (62), now that all the operators are defined, the modified evolution operator can then be written as

$$U' = S(I \otimes G)\mathcal{O}' = S(I \otimes G)\mathcal{O} \otimes I = S(\mathcal{O} \otimes G), \quad (68)$$

and the state of the system will evolve according to equation (63).

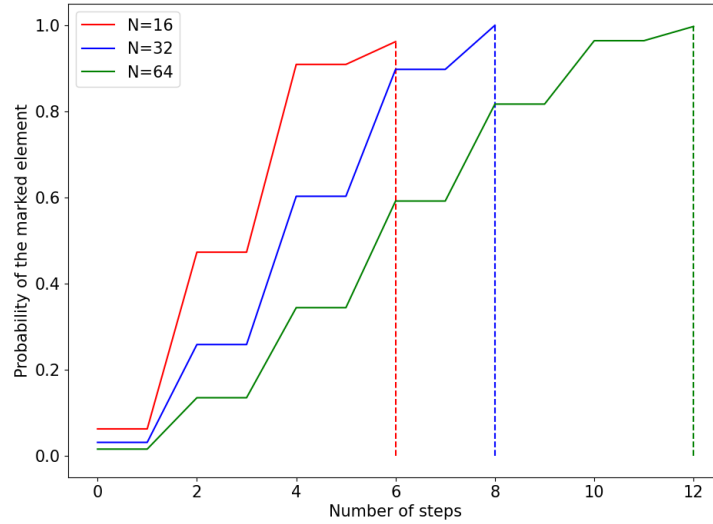


Figure 14: Probability of one marked element in the coined quantum walk search, as a function of the number of steps, for complete graphs of size $N = 16, 32$ and 64 .

As shown in Portugal (2018), maximum probability of the marked vertex is achieved after $\lfloor \frac{\pi}{2} \sqrt{N} \rfloor$ steps. Figure 14 is the result of coding and plotting the evolution of this probability distribution, for graphs of varying sizes. It shows that the probability is close to one at *approximately* the ideal steps, because of the discrete nature of the walk. The probability distributions have a stair-like shape, because transitions in this model only occur on even numbered time steps, because of the way the unmodified evolution operator was constructed.

The next section is devoted to the study of the search problem using the staggered quantum walk model. The algorithm is still discrete. However, since it does not use a coin, its Hilbert space will be much smaller. In the coined case, due to how the coin and shift operators were defined, for every qubit that represents the space of the walker, another qubit will be needed for the coin since, in the complete graph, each vertex is connected to all vertices. This means that for a N qubit walk, $2N$ qubits are required. Therefore, the staggered quantum walk will be better suited for running in a NISQ computer.

3.3 STAGGERED QUANTUM WALK

Defining the search problem in this model is similar to the coined quantum walk case. The oracle still inverts the sign of a certain state and amplifies it, and the system's state will still be described by equation (63). However, instead of using a coin, the staggered model takes advantage of the notions of cliques and tessellations, as was shown in chapter 2.3, which means the unmodified evolution operator has to be defined for an undirected complete graph.

As was previously seen, a complete graph is defined as a simple undirected graph where each pair of distinct vertices is connected by a unique edge. This is a special case, because this is the only connected graph that can be covered by a single tessellation, due to the fact that the graph is its own clique. The minimum tessellations required to cover this structures are defined by the one clique that encompasses all N vertices of the graph

$$\mathcal{T}_\alpha = \{\{0, 1, 2, \dots, N - 1\}\}. \quad (69)$$

The associated polygon can then be described as the balanced superposition of all the vertices in the graph

$$|\alpha\rangle = \frac{1}{\sqrt{N}} \sum_{v=0}^{N-1} |v\rangle. \quad (70)$$

The Hamiltonian, as defined in equation (17), is

$$H_\alpha = 2 \sum_0^1 |\alpha\rangle \langle \alpha| - I = 2 |\alpha_0\rangle \langle \alpha_0| - I. \quad (71)$$

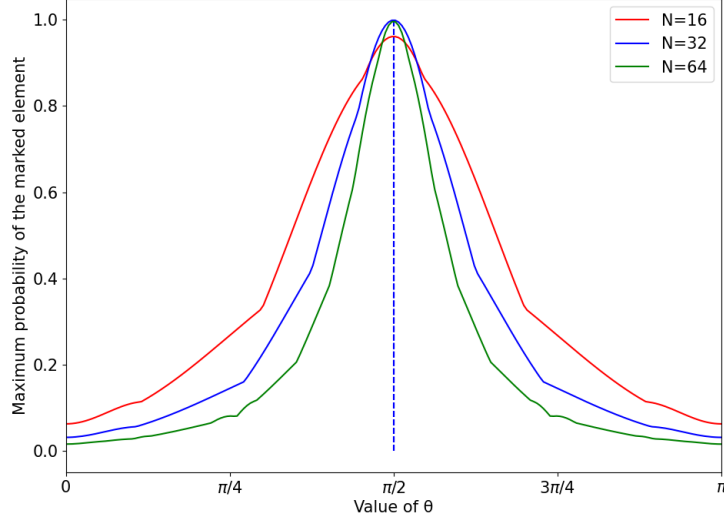


Figure 15: Maximum probability of the marked element as a function of the value of θ plotted from 0 to π , for complete graphs of size $N = 64, 128$ and 256 .

The unmodified evolution operator from equation (18)

$$U = e^{i\theta_k H_k} \dots e^{i\theta_2 H_2} e^{i\theta_1 H_1}, \quad (72)$$

reduces to the single Hamiltonian case

$$U = e^{i\theta H_\alpha}. \quad (73)$$

The choice of the value of θ is quite important, since maximum probability is achieved at $\theta = \frac{\pi}{2}$, as shown in figure 15.

Since $H_\alpha^2 = I$, equation (73) can be rewritten as

$$U = e^{-i\frac{\pi}{2} H_\alpha} = \cos \frac{\pi}{2} I + i \sin \frac{\pi}{2} H_\alpha = i H_\alpha = i(2 |\alpha_0\rangle \langle \alpha_0| - I). \quad (74)$$

Having defined the evolution operator associated to the complete graph, the next step is to use the oracle

$$\mathcal{O} = I_N - 2 |0\rangle \langle 0|, \quad (75)$$

to create the modified evolution operator associated with the search

$$U' = U\mathcal{O}. \quad (76)$$

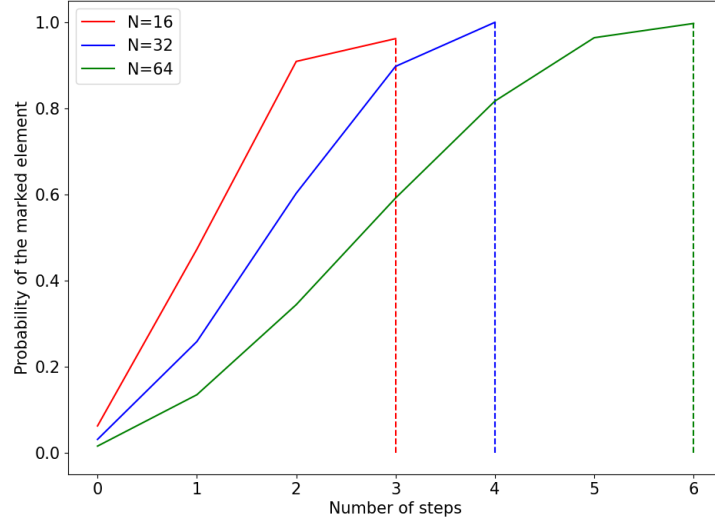


Figure 16: Probability of one marked element in the staggered quantum walk search, as a function of the number of steps, for complete graphs of size $N = 16, 32$ and 64 .

The walk achieves the same result as Grover’s algorithm after $\frac{\pi}{4}\sqrt{N}$ steps, as shown in figure 16. This plot also shows that the probabilities converge to 1 as N increases. Because time is discretized, deviations to the ideal number of steps will matter less for bigger values of N . Unlike Grover’s algorithm, however, the parameter θ can be changed in order to alter how many iterations are required to achieve maximum probability of the marked element. Combined with the fact that one has control over which structure this search problem is performed, the staggered quantum walk search is more general than Grover’s search, both being equivalent when a complete graph is considered and $\theta = \frac{\pi}{2}$.

Finally, the next section will present the search problem using the continuous-time quantum walk model. Since time is not discretized, a finer control over the evolution is possible. This will have significant impact when translating the algorithm to a quantum circuit, since it will be seen that circuit depth will not scale with an increase in time.

3.4 CONTINUOUS-TIME QUANTUM WALK

As was previously seen, the continuous-time quantum walk model is defined by an evolution operator obtained by solving Schrödinger’s equation

$$U(t) = e^{-iHt}. \tag{77}$$

The search problem requires introducing an oracle to the Hamiltonian, that will mark an arbitrary vertex m

$$H' = -\gamma L - \sum_{m \in M} |m\rangle \langle m|, \quad (78)$$

where M is the set of marked vertices. Since the complete graph is a regular graph, the operator can be rewritten in terms of the adjacency matrix plus the marked elements. Considering the case where only element $|0\rangle$ is marked, one gets

$$U'(t) = e^{-iH't} = e^{-i(-\gamma L - |0\rangle \langle 0|)t} = e^{-i(-\gamma A + \gamma D - |0\rangle \langle 0|)t} = e^{i\gamma(A + |0\rangle \langle 0|)t - i\gamma D t}. \quad (79)$$

The degree matrix is again $D = dI$, which means it will commute with $A + |0\rangle \langle 0|$ and become a global phase

$$U'(t) = e^{i\gamma(A + |0\rangle \langle 0|)t} e^{-i\gamma D t} = \phi(t) e^{i\gamma(A + |0\rangle \langle 0|)t}. \quad (80)$$

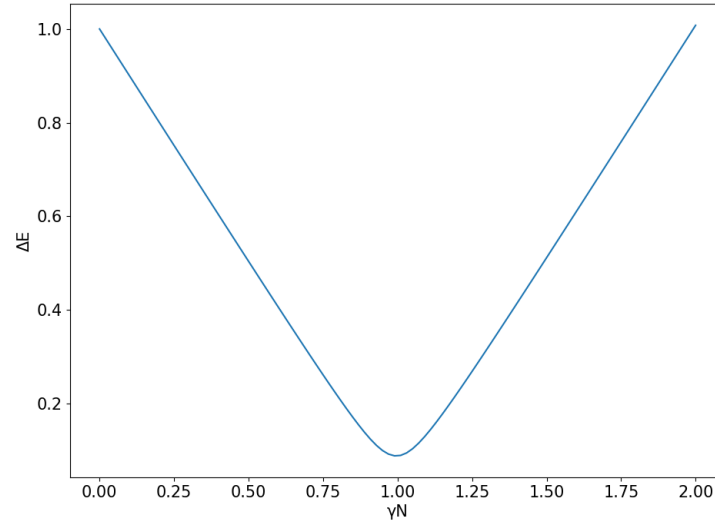


Figure 17: Value of the difference between the largest eigenvalue and the second largest plotted as a function of γN , for $N = 512$.

As shown by [Childs and Goldstone \(2004\)](#), the value of γ is crucial for the success of the search. As γ increases, the contribution of the marked element in the Hamiltonian decreases and, as γ approaches 0, the contribution of the adjacency matrix decreases. To find the

optimum value, the Hamiltonian can be rewritten by adding multiples of the identity matrix to the adjacency matrix

$$H' = -\gamma(A + NI) - |0\rangle\langle 0| = -\gamma N |s\rangle\langle s| - |0\rangle\langle 0|, \tag{81}$$

where $|s\rangle = \frac{1}{\sqrt{N}} \sum_i |i\rangle$. Now it is obvious that, for $\gamma = \frac{1}{N}$, the Hamiltonian becomes $H = -|s\rangle\langle s| - |0\rangle\langle 0|$. Its eigenstates are proportional to $|s\rangle \pm |w\rangle$ and eigenvalues are $-1 - \frac{1}{\sqrt{N}}$ and $-1 + \frac{1}{\sqrt{N}}$, respectively. This means that the evolution rotates from the state of balanced superposition to the marked vertex state in time $\frac{\pi}{\Delta E} = \frac{\pi}{2}\sqrt{N}$, where ΔE is the spectral gap. This is, as shown by Farhi et al. (2000), equivalent to Grover's algorithm.

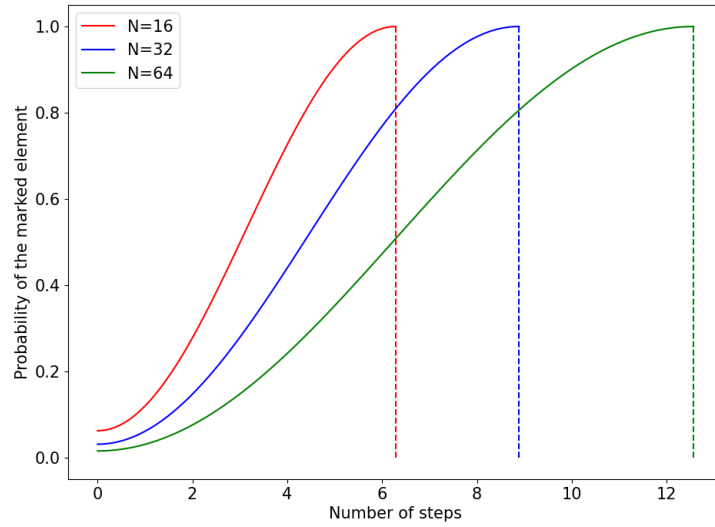


Figure 18: Probability of one marked element in the continuous quantum walk search, as a function of the number of steps, for complete graphs of size $N = 16, 32$ and 64 .

Plotting ΔE as a function of γN , as seen in figure 17, has a minimum at $\gamma N = 1$. The difference between the largest eigenvalue and second largest, plotted in the y-axis, is the smallest for a value of $\gamma N = 1 \implies \gamma = \frac{1}{N}$, which will correspond to the maximum probability for the marked vertex, in optimal steps.

Figure 18 shows the evolution of the probability of the marked vertex in time, which is continuous in this model. In contrast with previous models, the distributions are smooth and reach exactly one, since the walk is allowed to evolve for exactly the ideal time steps.

Again, this walk will require only as many qubits as needed to represent the space of the walker. Similarly to the staggered case, this model allows an adjustment to the γ parameter, that will affect the number of ideal steps. It also allows the choice of structure over which to perform the search, making it more general than the Grover algorithm as well. Another

interesting property is that, because time is treated as a continuous variable, the circuit associated will not scale in time. For the case without search, the circuit will be relatively small and somewhat resistant to noise. When considering the search problem, however, the introduction of the oracle and the dependency of the Suzuki-Trotter expansion will render the circuit less than ideal for NISQ implementation, as will be seen in the next chapter.

IMPLEMENTATIONS AND APPLICATIONS

This chapter is dedicated to the construction of quantum walk circuits using IBM's Software Development Kit, *Qiskit*, whose code is made publicly available in the Github repository¹. It is composed of two parts. The first one includes sections 4.1 through 4.3 and presents the circuits for the dynamics of each previously studied quantum walk model. The second part corresponds to section 4.4, where the search algorithm is studied for each model.

The first part of this chapter begins with section 4.1, where the coined quantum walk implementation based on the work of Douglas (2009) can be found. Here, the line graph is considered again, whose shift operation is composed of increment and decrement gates constructed with generalized CNOT gates. As seen in previous chapters, this model requires an extra qubit for the space of the coin that, when combined with all the operations required to implement the generalized CNOT gates, results in a circuit far too deep to be implemented in current NISQ computers, as was concluded at the end of this section. The staggered quantum walk circuit is presented in the following section, based on the work of Acasiete et al. (2020). This implementation still uses the notion of increment and decrement operations. However, since a coin was not required, the resulting circuit became much more NISQ-friendly. The first part is then concluded with section 4.3, where the continuous-time quantum walk circuit is implemented. The best results for the dynamics of the quantum walk were obtained for this case, due to the circulant graph approach that, unlike the previous discrete models, does not require extra iterations of the algorithm to represent time. Work by Qiang et al. (2016) firstly presented the circulant graph definition of this model, limited to the complete graph case, and the final part of this section greatly expands on this work by means of statistical analysis of the impact of the approximate quantum Fourier transform on a large collection of circulant graphs.

Finally, section 4.4 closes this chapter with the implementation of circuits for the search problem using quantum walks. It starts with the introduction of quantum searching by means of the circuit associated with Grover's algorithm, followed by the coined quantum walk, which produces the worst results due to the requirement of $2n$ qubits and swap gates

¹ <https://github.com/JaimePSantos/QWQiskit>

for the representation of the complete graph. Surprisingly, the best results were achieved for the staggered quantum walk search problem, since it produced the circuit with the least operations. The continuous-time quantum walk search was expected to produce the best results in this section also, but the introduction of the oracle together with the requirement of the Suzuki-Trotter expansion resulted in a circuit somewhat impacted by noise.

4.1 COINED QUANTUM WALK

Consider the example of a quantum walker on a discretely numbered cycle. It was seen that the evolution operator associated with such a system is, as defined in equation (6)

$$U = S(C \otimes I), \tag{82}$$

where S is a shift operator, defined in equation (5) as

$$S = |0\rangle \langle 0| \otimes \sum_{x=-\infty}^{x=\infty} |x+1\rangle \langle x| + |1\rangle \langle 1| \otimes \sum_{x=-\infty}^{x=\infty} |x-1\rangle \langle x|, \tag{83}$$

that increments or decrements the position of the walker according to the coin operator C .

Previously, this system was simulated in Python by coding its equations. Now, the focus is to study and implement a quantum circuit based on the work presented by Douglas (2009). This approach relies on multi-controlled CNOT gates, also known as generalized Toffoli gates, in order to shift the state of the walker by $+1$ or -1 , each with a probability associated with the chosen coin, as can be seen in figure 19. The generalized CNOT gates act on the

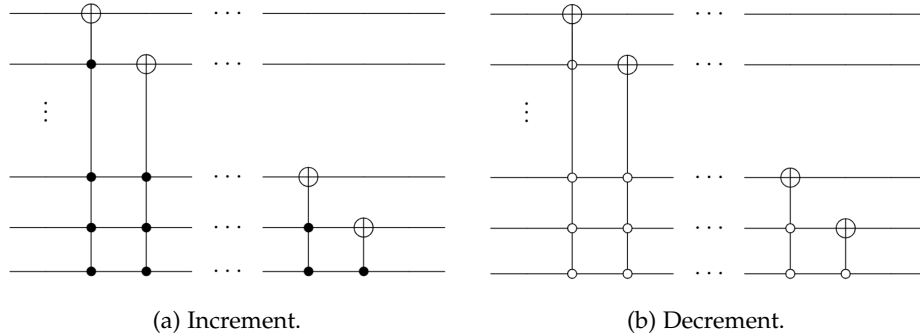


Figure 19: General circuits of the components of the shift operator for the coined quantum walk.

vertex states as a cyclic permutator, where each vertex state is mapped to an adjacent state. This can be seen as the walker moving left or right, in the line graph example.

The coin operator will simply be a Hadamard gate acting on a single qubit. For a graph of size $N = 8$, for example, $n = 3$ qubits are required to encode each vertex, and an extra qubit for the coin.

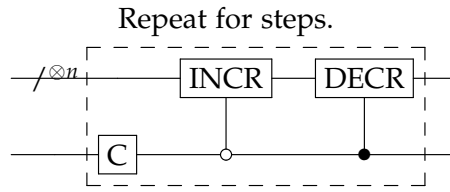


Figure 20: General circuit for the coined quantum walk.

The general circuit for the coined quantum walk is shown in figure 20. Note that this circuit limits the number of graph nodes to powers of 2, and an arbitrary implementation of 2^n nodes requires $n + 1$ qubits. However, it is possible to have any number of nodes, given that the proper correction is made, as was shown in the work of Douglas (2009). The method used for this correction is called *Gray Code Ordering* proposed by Slepoy (2006), whereby a certain arrangement of CNOT gates results in control states only differing by a single bit.

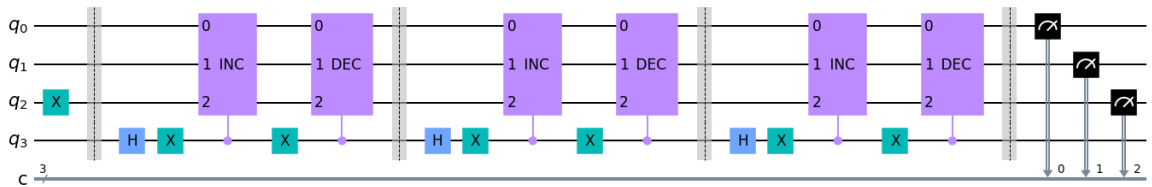


Figure 21: Qiskit circuit for the coined quantum walk, for a line graph of size $N = 8$ and initial condition $|\psi_0\rangle = |4\rangle$, with 3 steps and the Hadamard coin.

This circuit was implemented in Qiskit, as can be seen in figure 21. In this example, the increment and decrement sequence was applied three times on a graph of size $2^3 = 8$ nodes. The starting position of the walker was set to $\psi(0) = |4\rangle$, and the Hadamard coin was used.

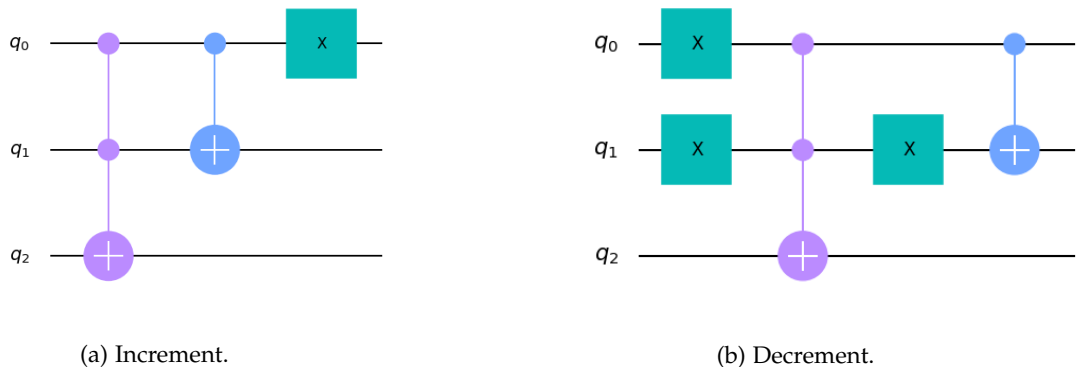


Figure 22: Qiskit circuits of the components of the shift operator for the coined quantum walk, for a line graph of size $N = 8$.

The first block after the barrier is the sequence of operations that will increment and decrement the state, as shown in figure 22. Note that, because the decrement gate is optimized, some X gates were removed. The generalized CNOT gates are implemented using Qiskit's *mcx* function, which decomposes these gates according to lemma 7.5 of Barenco et al. (1995) and work by Maslov (2016), to create CNOT gates up to four controls. For more generalized instances of the gate, the aforementioned Gray Code is used. The rest of the circuit is just the repetition of these operations as a function of the number of steps required.

Lastly, the circuit is measured. The results can be seen in figure 23. These results can be verified by calculating the time evolution of the wave function associated with the system

$$|\psi(0)\rangle = |4\rangle, \quad (84)$$

$$|\psi(1)\rangle = \frac{|0\rangle|x=3\rangle + |1\rangle|x=5\rangle}{\sqrt{2}}, \quad (85)$$

$$|\psi(2)\rangle = \frac{|0\rangle|x=2\rangle + |1\rangle|x=4\rangle + |0\rangle|x=4\rangle - |1\rangle|x=6\rangle}{2}, \quad (86)$$

$$|\psi(3)\rangle = \frac{|1\rangle|x=1\rangle - |0\rangle|x=3\rangle + 2(|0\rangle + |1\rangle)|x=5\rangle + |0\rangle|x=7\rangle}{2\sqrt{2}}. \quad (87)$$

Taking the modulus squared of the amplitudes associated with the states, confirms that the probability distribution associated with the QASM simulator, presented in figure 23 as the blue bar plot, is correct. However, the results obtained from running in IBM's *Toronto*

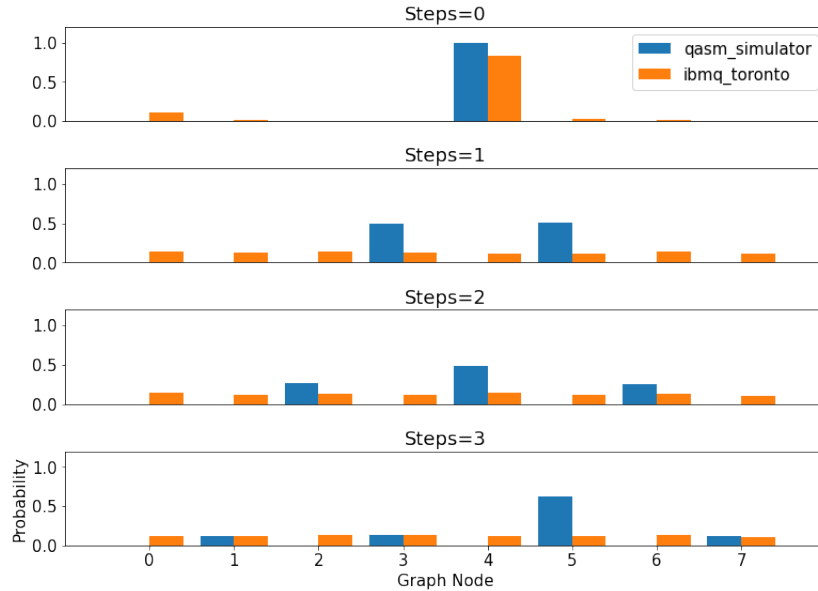


Figure 23: Probability distributions of the coined quantum walk for several steps in a line graph of size $N = 8$. The blue bar plot represents a circuit run in the QASM simulator, and the orange bar plot on IBM's *Toronto* backend.

backend are not satisfactory. This is because of the size of the circuit. Actually, the coined quantum walk model besides requiring an extra qubit for the coin, also needs a very large number of CNOT gates, more specifically 187, 372 and 569, for 1, 2 and 3 steps, respectively each of which have an average associated error of $1.284e - 2$ in this specific backend, at the time of this experiment. Note that this number may vary, depending on the transpiler seed used.

For a better error analysis, one can calculate the fidelity between the ideal distribution $p(x)$ and the experimental $q(x)$ using the formula

$$F(p, q) = \sum_{x=0}^{N-1} \sqrt{p(x)q(x)}, \quad (88)$$

where x is the vertex. For 0 steps, the obtained fidelity is approximately 0.91 which is very high, because the circuit is simply the initial condition. When the circuit is increased to 1 step the fidelity lowers to 0.49, due to the increase of CNOTs. However, for 2 and 3 steps, the fidelity increases again to approximately 0.63 due to the fact that the probability distribution in the simulator becomes more spread out with the increase of steps, meaning that the random uniform distribution obtained from the noisy experiments ran in IBM's backend will be closer to them than a highly localized distribution like in the case of 1 step.

In order to reduce the effects introduced by noise, the next chapter will present the circuit for the alternative discrete model, the staggered quantum walk. Besides avoiding an extra qubit for the coin, this model also does not require so many CNOT gates for each iteration.

4.2 STAGGERED QUANTUM WALK

As was discussed in section 2.3, the elements of each tessellation of a discretely numbered cycle can be described by states

$$|\alpha_x\rangle = \frac{|2x\rangle + |2x+1\rangle}{\sqrt{2}}, \quad (89)$$

$$|\beta_x\rangle = \frac{|2x+1\rangle + |2x+2\rangle}{\sqrt{2}}. \quad (90)$$

These states allow the construction of the Hamiltonians

$$H_\alpha = 2 \sum_{x=-\infty}^{+\infty} |\alpha_x\rangle \langle \alpha_x| - I, \quad (91)$$

$$H_\beta = 2 \sum_{x=-\infty}^{+\infty} |\beta_x\rangle \langle \beta_x| - I, \quad (92)$$

as in equations (24) and (25).

Following the implementation presented in the work of Acasiete et al. (2020), these operators can be rewritten in matrix form

$$H_\alpha = I \otimes X, \tag{93}$$

$$H_\beta = \begin{pmatrix} 0 & \cdots & 1 \\ \vdots & H_\alpha & \vdots \\ 1 & \cdots & 0 \end{pmatrix}, \tag{94}$$

which turn out to be very useful representations for the construction of the circuit.

As was shown in equation (26), the unitary evolution operator is

$$U = e^{i\theta H_\beta} e^{i\theta H_\alpha} = U_\beta U_\alpha, \tag{95}$$

knowing that

$$R_x(\theta) = e^{-\frac{i\theta X}{2}}, \tag{96}$$

then each of the evolution operators associated with the different tessellation Hamiltonians will be

$$U_\alpha = I \otimes R_x(\theta), \tag{97}$$

$$U_\beta = \begin{pmatrix} \cos \theta & \cdots & -i \sin \theta \\ \vdots & U_\alpha & \vdots \\ -i \sin \theta & \cdots & \cos \theta \end{pmatrix}. \tag{98}$$

Notice that U_β is simply a permutation of U_α , therefore it can be rewritten as

$$U_\beta = P^{-1} U_\alpha P, \tag{99}$$

where $P = \sum_x |x + 1\rangle \langle x|$.

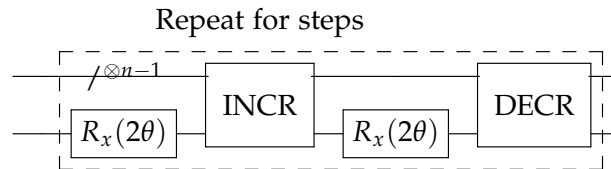


Figure 24: General circuit for the staggered quantum walk.

Remember from equation (83) and figure 19 that these permutation operators can be implemented as increment and decrement gates, defined in the work of Douglas (2009).

Therefore, the circuit for the staggered quantum walk on the line can be built as shown in figure 24.

The next step is to implement the circuit in Qiskit, in order to test it in a real quantum computer. Here, the walk will take place in a cyclic graph with 8 elements, which means that 3 qubits will be required, as shown in figure 25. The circuit starts with a Pauli-X gate in

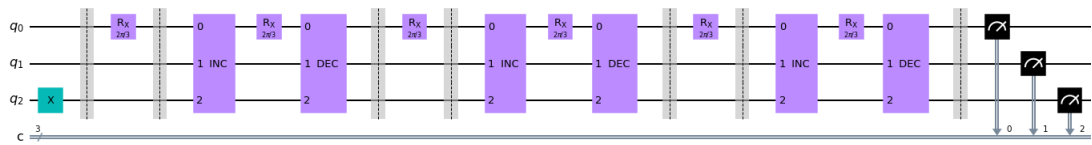


Figure 25: Qiskit circuit for the staggered quantum walk, for a line graph of size $N = 8$ and initial condition $|\psi_0\rangle = |4\rangle$, with 3 steps.

the third qubit so that $|\psi_0\rangle = |4\rangle$. The following operation is a rotation in the X basis, where $\theta = \frac{\pi}{3}$, since it was seen in figure 7 that this value of θ maximizes the propagation of the walk. Finally, U_β is applied, making use of the increment and decrement gates defined in figure 22. Note that now, because this model does not require a coin, these gates do not need to be controlled, meaning that the largest multi-controlled NOT gate will not be needed, making the circuit more NISQ-friendly. This procedure is repeated 3 times, and the resulting probability distributions after measurement are depicted in figure 26.

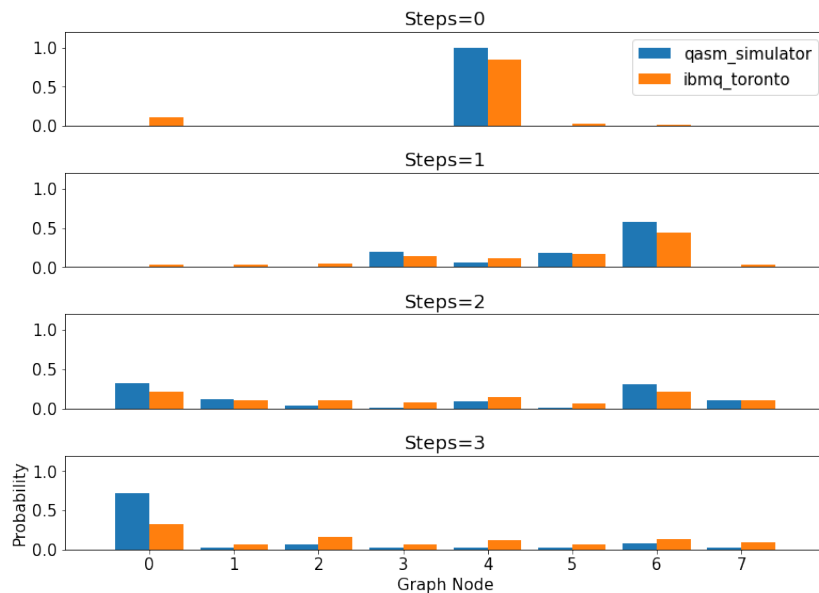


Figure 26: Probability distributions of the staggered quantum walk for several steps in a line graph of size $N = 8$. The blue bar plot represents a circuit run in the QASM simulator, and the orange bar plot on IBM’s Toronto backend.

Analyzing the figure, it is clear that this model is much better suited for running in current NISQ hardware. Even though the probability distribution was somewhat affected by noise,

the dynamics of the walk is relatively unaffected in the Toronto backend experiment. This is mainly due to the much smaller number of CNOT gates, when compared to the last model. Now, for 1, 2 and 3 steps, the gate count was 21, 37 and 64, respectively.

The highest fidelity was achieved for 2 steps, with a value of approximately 0.95, and the remaining steps ranging from 0.91 to 0.92. Again, it may seem counter-intuitive that a higher fidelity is achieved for a larger circuit, compared to 0 steps for example, but this is again due to the balance of circuit size and spread of the probability distribution.

Nevertheless, because this discrete model requires ever more operations with the increase of steps, it will eventually become intractable for NISQ technology. This justifies that the next model studied in this work is one where the circuit will be constant in time.

4.3 CONTINUOUS-TIME QUANTUM WALK

As was seen in section 2.4, the unitary evolution operator of this model is defined as

$$U(t) = e^{-iHt} = e^{i(\gamma L)t} = e^{i\gamma(A-D)t}. \quad (100)$$

Considering a regular graph, this operator can be rewritten as

$$U(t) = \phi(t)e^{i\gamma(A)t}, \quad (101)$$

where $\phi(t)$ is a global phase and A is the adjacency matrix associated with the graph.

In this section, the study will focus on the circuit implementation of this walk in a cycle graph, where the associated adjacency matrix will be defined using a circulant matrix. The motivation behind this choice was that the circulant graph class can be easily diagonalized with the quantum Fourier transform, which means it has a straightforward implementation in Qiskit.

The class of circulant graphs is defined by a circulant adjacency matrix such that

$$A = \begin{pmatrix} c_0 & c_{N-1} & \cdots & c_3 & c_2 \\ c_1 & c_0 & c_{N-1} & & c_3 \\ \vdots & c_1 & c_0 & \ddots & \vdots \\ c_{N-2} & & \ddots & \ddots & c_{N-1} \\ c_{N-1} & c_{N-2} & \cdots & c_1 & c_0 \end{pmatrix}, \quad (102)$$

where $c_k = 1$ if the vertices are connected, and 0 otherwise. In order to generate the proper circulant graphs, restrictions on this matrix are in order. Firstly, $c_0 = 0$, since self-loops are not part of the structure. Secondly, the matrix must be symmetric, therefore $c_{n-j} = c_j$.

These matrices can be fully described by their first columns

$$v_1 = [c_0, c_1, \dots, c_{N-2}, c_{N-1}]^T, \quad (103)$$

with a discrete convolution operator performing cyclic permutations of c , on each column, known as the *deque* operator. For example,

$$Dv_1 = [c_{N-1}, c_0, \dots, c_{N-3}, c_{N-2}]^T = v_2. \quad (104)$$

More specifically, for the cycle case

$$Dv_1 = D[0, 1, 0, \dots, 0, 1]^T = [1, 0, 1, 0, \dots, 0, 0]^T = v_2. \quad (105)$$

The eigenvalues of a circulant matrix are given by

$$\lambda_p = c_0 + \sum_{q=1}^{n-1} c_{N-q} \omega^{pq}, \quad (106)$$

and the eigenvectors by

$$|\varphi_p\rangle = \frac{1}{\sqrt{n}} \sum_{q=0}^{n-1} \omega^{pq}. \quad (107)$$

This given, it is possible to construct an operator that diagonalizes the circulant matrix through the eigenvectors, which is useful for constructing the circuit. For this purpose, the quantum Fourier transform can be used. It is defined by

$$F = \frac{1}{\sqrt{N}} \sum_{p,q} \omega^{pq} |p\rangle \langle q|, \quad (108)$$

and further reading can be done in appendix A.2. The adjacency matrix of a circulant graph is then diagonalized such that

$$A = F^\dagger \Lambda F, \quad (109)$$

where Λ is a diagonal operator that encodes the eigenvalues, i.e.

$$\Lambda = \sum_j \lambda_j |j\rangle \langle j|. \quad (110)$$

The unitary operator of the walk can then be rewritten as

$$U = F^\dagger e^{i\gamma\Lambda t} F, \quad (111)$$

where

$$e^{i\gamma\Lambda t} = \sum_j e^{i\gamma\lambda_j t} |j\rangle \langle j|. \tag{112}$$

This representation is very easily translatable to a quantum circuit, as shown in figure 27.

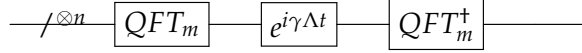


Figure 27: General circuit for the continuous-time quantum walk.

The circuit can now be constructed making use of the *diagonal* function provided by Qiskit, which decomposes diagonal operators based on the method presented in theorem 7 of Shende et al. (2006). The other tool used was the quantum Fourier transform (QFT) also provided by the Qiskit package. Figure 28 shows the implementation of the circuit for $2^3 = 8$ graph nodes.

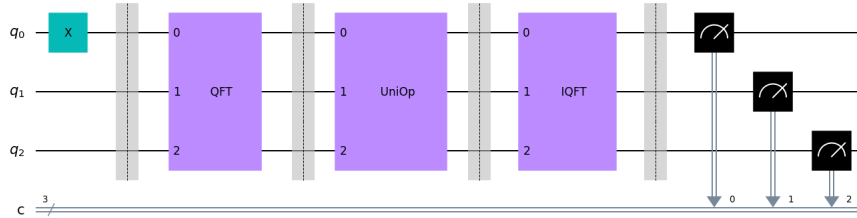


Figure 28: Qiskit circuit for the continuous-time quantum walk, for a line graph of size $N = 8$ and initial condition $|\psi_0\rangle = |4\rangle$, for time t .

The quantum Fourier transform circuit, presented in figure 29, is well known. The inverse QFT is similarly constructed by changing the signs of the angles of rotation associated with the QFT.

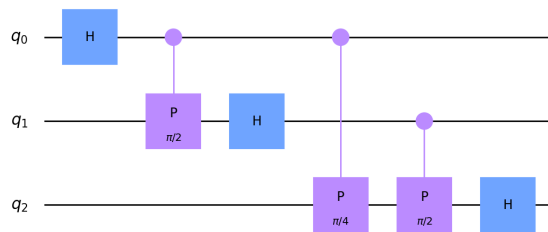


Figure 29: Qiskit circuit of the quantum Fourier transform for a line graph of size $N = 8$.

The circuit associated with the diagonal operator is shown in figure 30. Furthermore equation (111) says that time is simply a constant inside the exponential, which means that

the diagonal operator’s circuit will not need extra operations when increasing time, only when in size. It will simply require different rotations and it will differ in global phase. This is an advantage when comparing to previous discrete models, where each extra step required another increment and decrement gates.

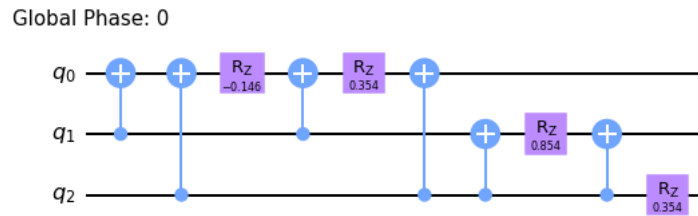


Figure 30: Qiskit circuit of the diagonal operator associated with the adjacency matrix, for a line graph of size $N = 8$.

Finally, the circuit was measured. The resulting probability distributions can be seen in figure 31.

The dynamics of the walk, when ran on the Toronto backend, is closer to the simulation than the previous examples. Now, the size of the circuit does not scale with time, and 29 CNOT gates were required to implement the walk for $t = 1, 2$ and 3.

A fidelity of approximately 0.97 was achieved for $t = 3$. For $t = 0, 1, 2$, the respective fidelities were 0.96, 0.90, 0.92, which are small improvements when compared to the staggered quantum walk. Fidelity also stays relatively constant with increasing time, making this type

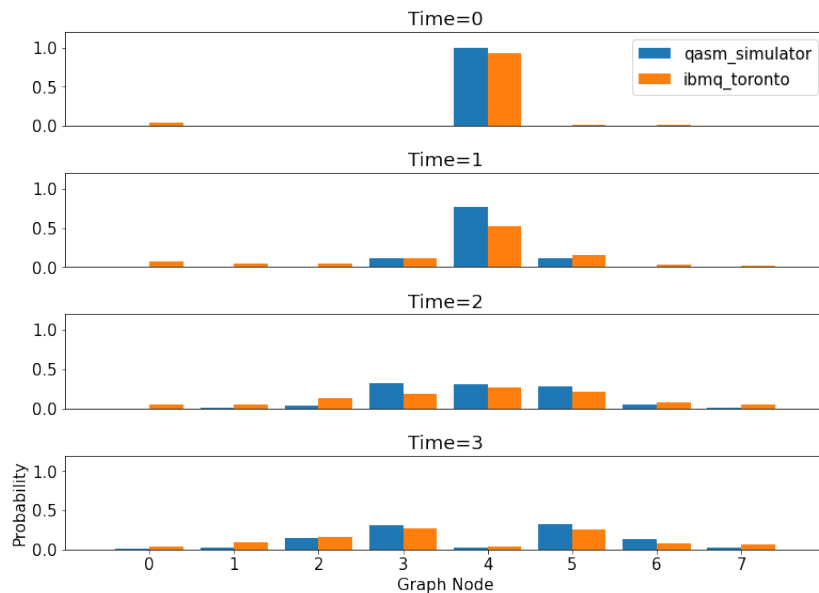


Figure 31: Probability distributions of the continuous-time quantum walk for several steps in a line graph of size $N = 8$. The blue bar plot represents a circuit run in the QASM simulator, and the orange bar plot on IBM’s Toronto backend.

of circuit well suited for studying the dynamics of the continuous-time quantum walk.

Further Experiments

Another improvement, presented in the accepted paper by Santos et al. (2021), can be made to this model resorting to the approximate quantum Fourier transform (AQFT). The AQFT, proposed by Coppersmith (2002), is achieved through the modification of the regular quantum Fourier transform circuit, as defined in appendix A.2, by removing the phase-shift operations between the most distant qubits. This can be implemented in Qiskit by providing the QFT function the approximation degree.

Each experiment was performed 10 times, with 3000 shots each, in order to extract substantial statistical data, using the confidence interval of 95%. The average fidelity between the ideal $p(x, t)$ and the experimental $q(x, t)$ distributions is again calculated using

$$F(p, q) = \frac{1}{10} \sum_{i=1}^{10} \sum_{x=0}^{N-1} \sqrt{p(x, t)q(x, t)}, \quad (113)$$

which is a simple modification of equation (88).

For this section, not only is the cyclic graph considered, but also a considerable number of other circulant graph, as is shown in figure 32. The numbering of graphs follows the rule that G_k will have entries $c_k, \dots, c_1 = 1$ and $c_{n-k}, \dots, c_{n-1} = 1$, and the remaining elements are 0. This way, it is possible to systematically construct circulant graphs varying from sparse to dense.

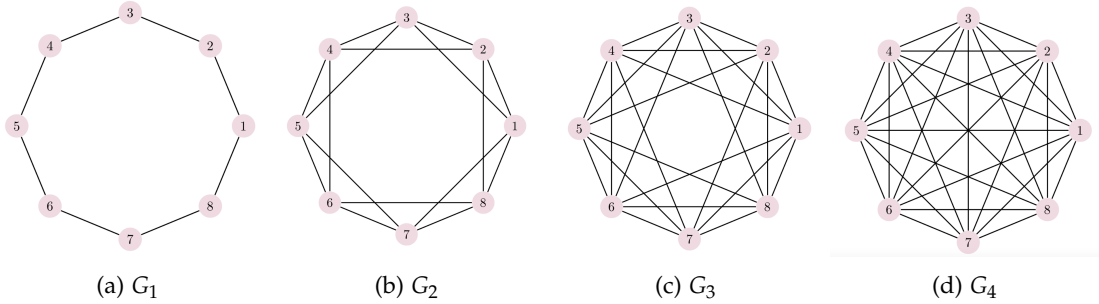


Figure 32: Circulant graphs G_k for $N = 8$ elements.

Starting with a smaller $N = 2^2 = 4$ case, two non-isomorphic circulant graphs can be built. G_1 corresponds to the cycle graph, and G_2 to the complete graph. Table 1 shows the achieved average fidelities, which were calculated with equation (113). Comparing to the complete graph case presented in Qiang et al. (2016), where a fidelity of 0.967 ± 0.003 was obtained, it is possible to see that the implementation presented here slightly outperforms it in terms of fidelity.

$m \backslash G$	G_1	G_2
0	0.98 ± 0.01	0.99 ± 0.01
1	0.98 ± 0.02	0.993 ± 0.006

Table 1: Fidelity of quantum state with $N=4$, backend *Toronto*, and $t=1$.

For the $N = 2^3 = 8$ case, table 2 shows that state fidelity is greater as graph connectivity increases, and as m increases. This is due to the fact that a greater m implies a smaller circuit, but also an increase in error. However, graphs have less distinct eigenvalues as they are more connected, which means that a higher degree of approximation of the QFT will generally introduce less errors, while keeping the circuit depth lower.

$m \backslash G$	G_1	G_2	G_3	G_4
0	0.80 ± 0.01	0.92 ± 0.02	0.968 ± 0.007	0.965 ± 0.006
1	0.894 ± 0.007	0.95 ± 0.01	0.98 ± 0.01	0.973 ± 0.008
2	0.852 ± 0.009	0.955 ± 0.004	0.985 ± 0.003	0.990 ± 0.002

Table 2: Fidelity of quantum state with $N=8$, backend *Toronto*, and $t=1$.

Finally, table 3 presents the $N = 2^4 = 16$ case. Here, the behavior is similar to the previous case up to graph G_5 , meaning that higher graph connectivity and larger m will result in higher fidelity. However, graphs G_6 , G_7 and G_8 , even though highly connected and with relatively low depth, present lower fidelity. This seems to contradict the results in table 2.

$m \backslash G$	G_1	G_2	G_3	G_4	G_5	G_6	G_7	G_8
0	0.47 ± 0.03	0.61 ± 0.02	0.78 ± 0.02	0.86 ± 0.01	0.86 ± 0.01	0.70 ± 0.04	0.54 ± 0.03	0.49 ± 0.04
1	0.50 ± 0.03	0.63 ± 0.03	0.79 ± 0.03	0.87 ± 0.02	0.85 ± 0.03	0.70 ± 0.03	0.55 ± 0.05	0.50 ± 0.04
2	0.55 ± 0.03	0.71 ± 0.03	0.83 ± 0.02	0.90 ± 0.01	0.89 ± 0.02	0.75 ± 0.02	0.62 ± 0.04	0.59 ± 0.06
3	0.60 ± 0.03	0.70 ± 0.02	0.85 ± 0.01	0.92 ± 0.01	0.91 ± 0.01	0.80 ± 0.03	0.71 ± 0.04	0.69 ± 0.04

Table 3: Fidelity of quantum state with $N=16$, backend *Toronto*, and $t=1$.

However this behavior can be explained due to the fact that the probability distribution of the dynamics of the walk on these structures is highly concentrated in a small number for vertices. Considering that the size of the circuit starts to push the limits of NISQ computers, it is expected that the spreading out of the probability distribution due to the effects of noise produces a lower fidelity. Nonetheless, the increase of m still has a positive impact on the fidelity of these circuits, which means that the reduction in circuit size will indeed produce better results.

4.4 IMPLEMENTING SEARCH ALGORITHMS IN QISKIT

4.4.1 Grover's Algorithm

As discussed in section 3.1, Grover's algorithm is a quantum process to address unstructured search problems. Consider the case of finding element x_0 out of an unordered list of size N . For the worst case scenario, a classical algorithm would need to check every element of the list, therefore requiring N steps.

The first stage of Grover's algorithm is to create an uniform superposition of all states in the system

$$|\psi_0\rangle = \frac{1}{\sqrt{N}} \sum_{x=0}^{N-1} |x\rangle. \quad (114)$$

The next stage is the application of the Grover iteration process, which starts with an oracle that adds a negative phase to the solution states

$$\mathcal{O} |x\rangle = (-1)^{f(x)} |x\rangle. \quad (115)$$

This operator can be seen as an identity matrix with negative entries corresponding to the solution states. The operator can be rewritten as

$$\mathcal{O} = I - 2 \sum_{m \in M} |m\rangle \langle m|. \quad (116)$$

where I is the identity matrix and M is a set of solutions where $f(m) = 1$, and 0 otherwise. The matrix associated with this operator is

$$\mathcal{O} = \begin{pmatrix} (-1)^{f(0)} & 0 & \cdots & 0 \\ 0 & (-1)^{f(1)} & \cdots & 0 \\ \vdots & 0 & \ddots & \vdots \\ 0 & 0 & \cdots & (-1)^{f(N-1)} \end{pmatrix}. \quad (117)$$

The second part of the iteration is an amplitude amplification process through the diffusion operator

$$\mathcal{D} = (2 |\psi_0\rangle \langle \psi_0| - I) = H^{\otimes n} (2 |0\rangle \langle 0| - I) H^{\otimes n}. \quad (118)$$

The unitary operator that describes the Grover iteration process will then be

$$\mathcal{U} = \mathcal{D}\mathcal{O}. \quad (119)$$

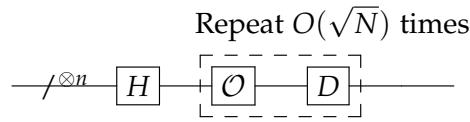


Figure 33: General circuit for the Grover search.

As previously discussed, this iteration process will be repeated several times, depending on the number of elements. Optimal probability of success in finding a single solution will be reached after $\lfloor \frac{\pi}{4} \sqrt{N} \rfloor$ steps, and $\lfloor \frac{\pi}{4} \sqrt{\frac{N}{K}} \rfloor$ for K solutions, which amounts to a quadratic gain when compared to the classical case. The general Grover circuit can then be constructed as shown in figure 33.

Consider the 3 qubit case, where $N = 8$ and solution state $|4\rangle$. The optimal number of iterations is approximately 2. Figure 34 depicts the circuit for 3 iterations implemented in Qiskit.

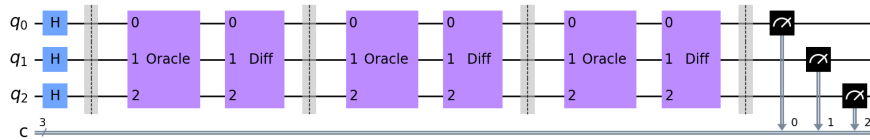


Figure 34: Qiskit circuit for the Grover algorithm, for a search space of size $N = 8$ and 3 steps.

The system starts with the creation of an uniform superposition state, by applying Hadamard gates to each qubit. Immediately following the barrier, the first operator of the

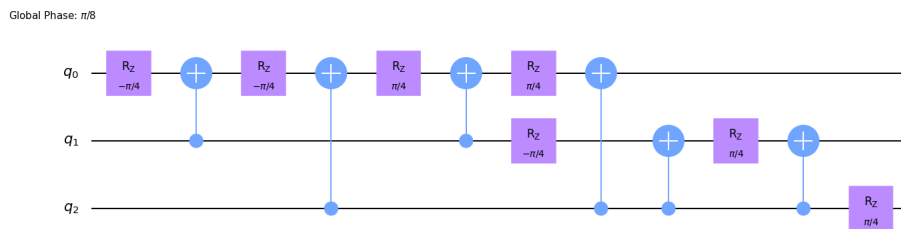


Figure 35: Qiskit circuit of the diagonal oracle operator for a search space of size $N = 8$ and marked element $|m\rangle = |4\rangle$.

iteration process is the oracle, which is shown in figure 35. Because the oracle operator is simply the identity matrix with negative entries corresponding to the solution states, it can be simply translated into a circuit through the *diagonal* function in Qiskit.

The last part of the iteration is the diffusion operator, whose circuit is shown in figure 36. Comparing equations (116) and (118), it is easy to see why figures 35 and 36 are so similar.

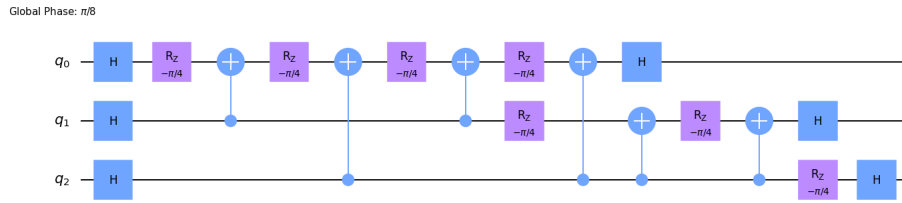


Figure 36: Qiskit circuit of the diagonal Grover diffusion operator for a search space of size $N = 8$.

The diffusion circuit will simply be the oracle circuit for state $|0\rangle$, placed between Hadamard operations.

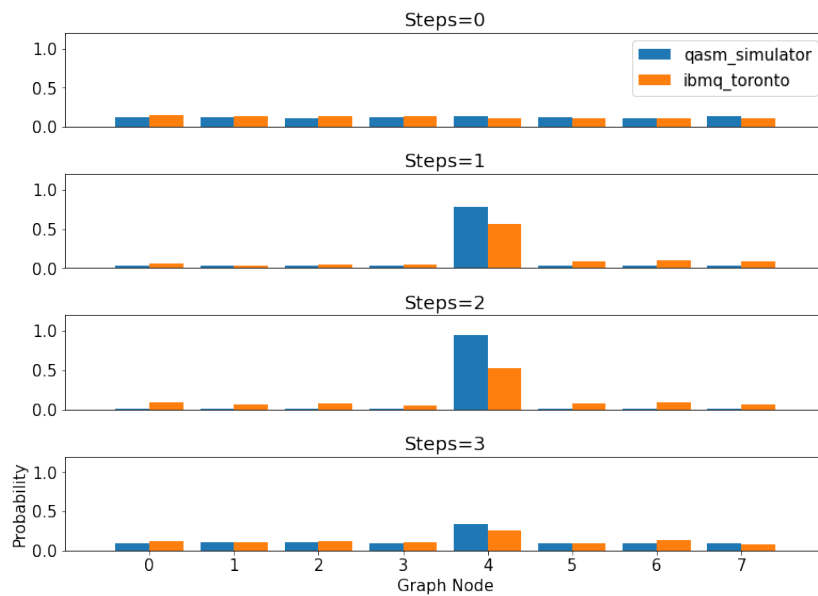


Figure 37: Probability distributions of the Grover search algorithm for several steps, in a search space of size $N = 8$. The blue bar plot represents a circuit run in the QASM simulator, and the orange bar plot on IBM’s Toronto backend.

The results of measurement are shown in figure 37. As expected, the maximum probability for the marked element was reached after 2 iterations, on the simulator, and it decreases in subsequent steps. However, the experimental result from the Toronto backend presents maximum probability for the marked element for 1 step, with a fidelity of 0.96. The optimal number of steps, in contrast, has a lower fidelity of 0.89. This is because as the number of steps increases, so does the circuit depth, more specifically the number of CNOT gates for 1, 2 and 3 steps were 19, 45 and 60, respectively. Therefore, the circuit does not achieve the maximum probability after 2 steps due to the effects introduced by noise.

Despite this, the results are satisfactory when taking into account the properties of NISQ computers. The following sections will present the search problem adapted to several quantum walk models.

4.4.2 Searching with a Coined Quantum Walk

Following the structure of section 3.2, this section expands the coined quantum walk model into a circuit for searching.

The modified unitary evolution operator is

$$U' = S(\mathcal{O} \otimes G), \tag{120}$$

as was defined in equation (68), where S is the flip-flop shift operator, \mathcal{O} is the oracle operator and G is the Grover diffusion as a coin operator.

Consider the case of a complete graph, where every vertex is adjacent to one another. The general quantum circuit to implement this, as shown in figure 38, will require n qubits to represent the state of the walker and n qubits for the state of the coin. The shift operator was constructed based on the work of Douglas (2009), where the state of the walker is flip-flopped with the state of the coin with a swap operation.

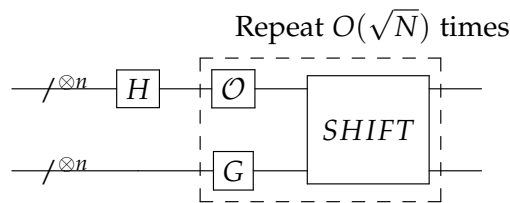


Figure 38: General circuit for the search problem using the coined quantum walk model.

This was implemented in Qiskit, for a graph of size $N = 2^3 = 8$, which means 6 qubits will be required. For the case of one marked element, the number of iterations that maximizes the amplitude of the solution state is $\lfloor \frac{\pi}{2} \sqrt{N} \rfloor$. Figure 39 shows the circuit for 5 iterations of the walk.

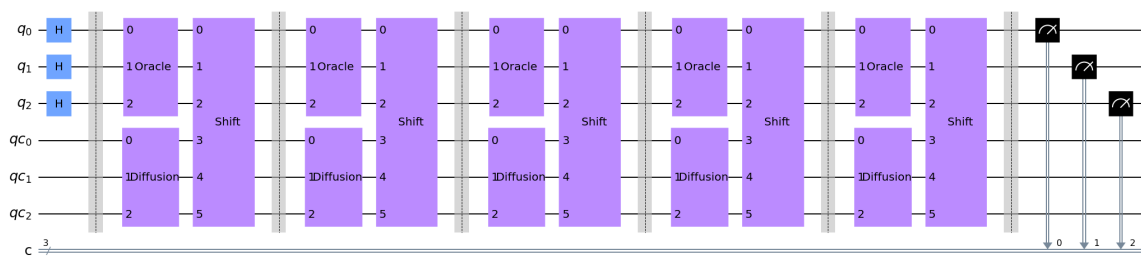


Figure 39: Qiskit circuit for the search problem using the coined quantum walk model, for a complete graph of size $N = 8$ and with 5 steps.

The circuit starts in a uniform superposition of the states corresponding to the vertices of the graph. The first step of the iteration is the oracle. This operator flips the amplitude of

the vertex state $|4\rangle$, and can be translated into a circuit making use of the Qiskit's *diagonal* function, as shown in figure 40. It is the same oracle used in the Grover search of figure

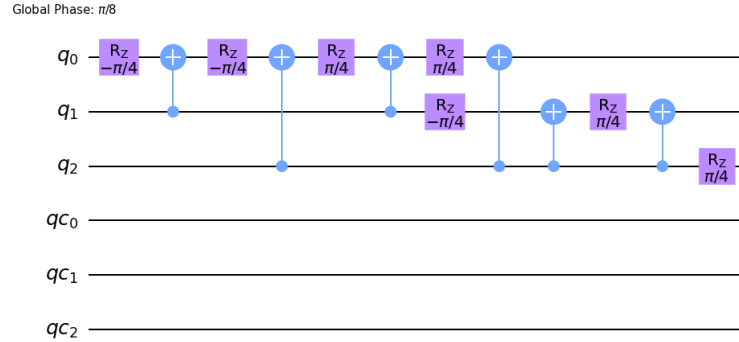


Figure 40: Qiskit circuit of the diagonal oracle operator in the coined quantum walk search problem, for a complete graph of size $N = 8$, with marked element $|m\rangle = |4\rangle$.

35, but in the coined quantum walk model it is only applied to the states associated with the position of the walker. The states associated with the coin space of the walk will be transformed according to Grover's diffusion of figure 36, as seen in figure 41.

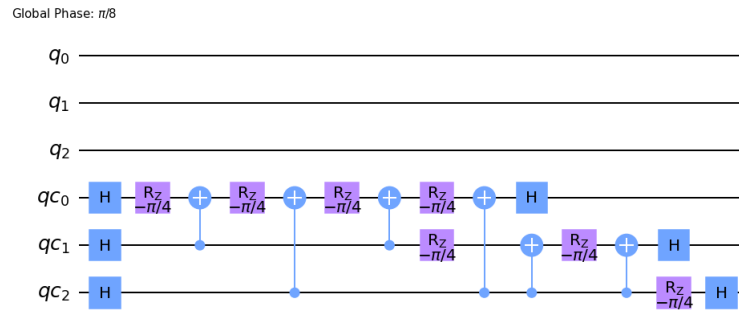


Figure 41: Qiskit circuit of the diagonal diffusion operator in the coined quantum walk search problem, for a complete graph of size $N = 8$.

The final part of the iteration is the shift operator, as represented in figure 42. The flip-flop shift operator was defined in equation (64) as

$$S |v1\rangle |v2\rangle = |v2\rangle |v1\rangle, \tag{121}$$

where $|v1\rangle$ represents the position of the walker and $|v2\rangle$ is the state of the coin. Making use of the swap gate, this operator can be implemented as in figure 42.

Lastly, measurements were performed. The results are plotted in figure 43. Maximum probability of the marked element was reached after 4 steps in the simulator. Extra steps reduce that probability. The resulting probability distribution from the Toronto backend is again unsatisfactory for the coined quantum walk model, with fidelities ranging from 0.58

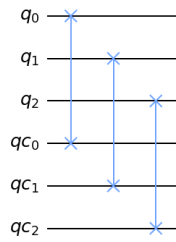


Figure 42: Qiskit circuit of the flip-flop shift operator in the coined quantum walk search problem, for a complete graph of size $N = 8$.

for 4 steps, to 0.75 for 2 steps. This is expected, since the complete graph representation requires N extra qubits for the coin, and swap operations which are decomposed into 3 CNOT gates each, resulting in 92, 210 and 261 CNOT operations for 2, 4 and 5 steps, respectively. The optimal number of steps that maximizes the probability of the marked element is also a contributing factor to the size of the circuit, requiring more iterations to achieve the same probability when compared to Grover’s search discussed above.

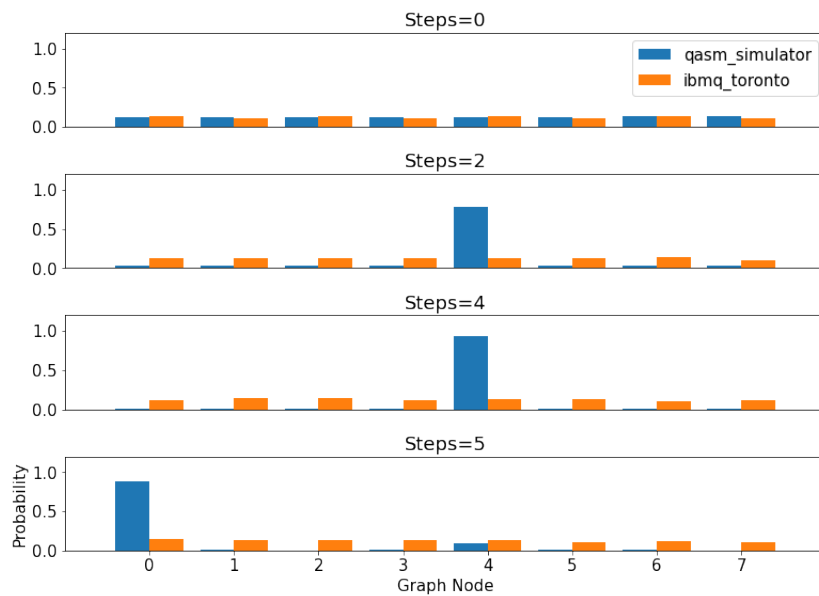


Figure 43: Probability distributions of the coined quantum walk search problem for several steps, in a complete graph of size $N = 8$. The blue bar plot represents a circuit run in the QASM simulator, and the orange bar plot on IBM’s Toronto backend.

As mentioned previously, other models of the quantum walks that do not require coins or iterations will be studied in the following sections, in the context of the searching problem. The staggered quantum walk, for example, should be able to present better results when ran in a NISQ computer, considering the smaller Hilbert space due to its coinless nature.

4.4.3 Searching with a Staggered Quantum Walk

As discussed in section 3.3, the staggered quantum walk on a complete graph requires a single tessellation with associated polygon

$$|\alpha\rangle = \frac{1}{\sqrt{N}} \sum_{x=0}^{N-1} |x\rangle. \tag{122}$$

The Hamiltonian will then be

$$H_\alpha = 2 \sum_0^1 |\alpha\rangle \langle \alpha| - I = H^{\otimes n} (2 |0\rangle \langle 0| - I) H^{\otimes n} = H^{\otimes n} \mathcal{O}_0 H^{\otimes n}, \tag{123}$$

which is equivalent to the Grover diffusion operator. Therefore, it can be implemented in a similar fashion.

The evolution operator for the staggered quantum walk on the complete graph can then be defined as

$$U = e^{i\theta H_\alpha} = e^{i\theta(H^{\otimes n} \mathcal{O}_0 H^{\otimes n})} = H^{\otimes n} e^{i\theta \mathcal{O}_0} H^{\otimes n}. \tag{124}$$

This is a very useful representation since the exponent part of the operator is a diagonal matrix, which means that implementing the circuit in Qiskit is straightforward.

Now that the staggered quantum walk associated with the complete graph is defined, what remains to be done is to add an oracle to the evolution operator, as was done in equation (76),

$$U' = U\mathcal{O}, \tag{125}$$

where

$$\mathcal{O} = I_N - 2 \sum_{m \in M} |m\rangle \langle m|, \tag{126}$$

and M is the set of marked elements.

The general circuit for implementing the staggered quantum walk search problem in a complete graph is shown in figure 44. Since only one tessellation is required, there is no

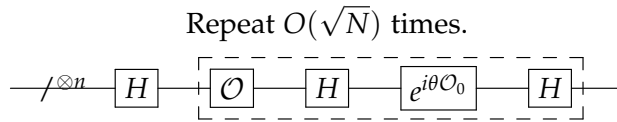


Figure 44: General circuit for the search problem using the staggered quantum walk model.

need for the Suzuki-Trotter approximation. However, several iterations will be needed in order to achieve the maximum probability for the marked vertex. As the staggered quantum

walk search algorithm a complete graph is equivalent to Grover’s algorithm, the optimum number of steps will also be $\lfloor \frac{\pi}{4} \sqrt{\frac{N}{K}} \rfloor$, where K is the number of solutions.

Consider the case of $N = 8$ and one marked vertex, $|m\rangle = |4\rangle$. The number of steps that maximizes the probability of the marked element is $\lfloor \frac{\pi}{4} \sqrt{\frac{8}{1}} \rfloor = 2$. Translating to Qiskit, $n = 3$ qubits will be needed and the circuit will be as in figure 45. Similar to previous examples,

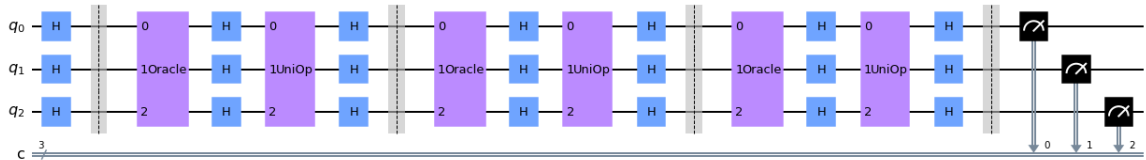


Figure 45: Qiskit circuit for the search problem using the staggered quantum walk model, for a complete graph of size $N = 8$, with 3 steps and a value of $\theta = \frac{\pi}{2}$.

the circuit begins with a uniform superposition built by the Hadamard gates. The next operation is the oracle, which was implemented through the use of Qiskit’s *diagonal* function, producing a circuit similar to the one in figure 35.

Next, an analogue to Grover’s diffusion operator is applied, where the operation named *UniOp* is a diagonal matrix, easily translated to Qiskit, as shown in figure 46. This circuit is

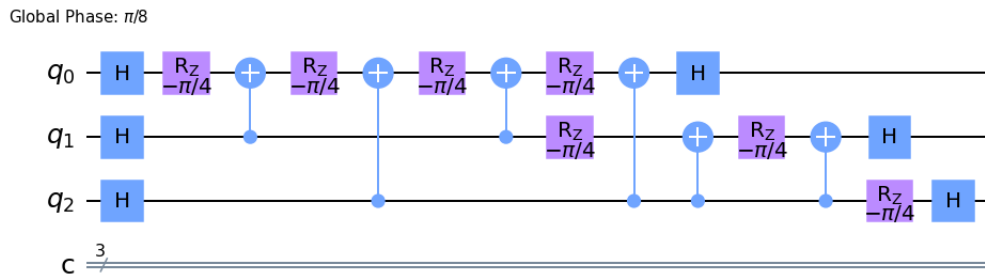


Figure 46: Qiskit circuit of the diagonal diffusion operator in the staggered quantum walk search problem, for a complete graph of size $N = 8$ and a value of $\theta = \frac{\pi}{2}$.

very similar to the one in figure 36, the difference being that in the staggered quantum walk search model one can control the value of θ , as seen in equation (124). This influences how fast maximum probability of the marked element is achieved. Since Grover’s algorithm is optimal, a value of $\theta = \frac{\pi}{2}$ yields a diffusion circuit equal to the one in figure 36, implying that the staggered quantum walk is a more general model of quantum searching.

Finally, measurement is performed and the results for several steps of the walk are shown in figure 47. The circuit for each step of the walk was run both in the QASM simulator and IBM’s backend named Toronto. The experiment was performed with 3000 shots in both cases, and the probability distributions show that this model is indeed more suited for a NISQ computer than the previous case. However, unlike the simulator, maximum

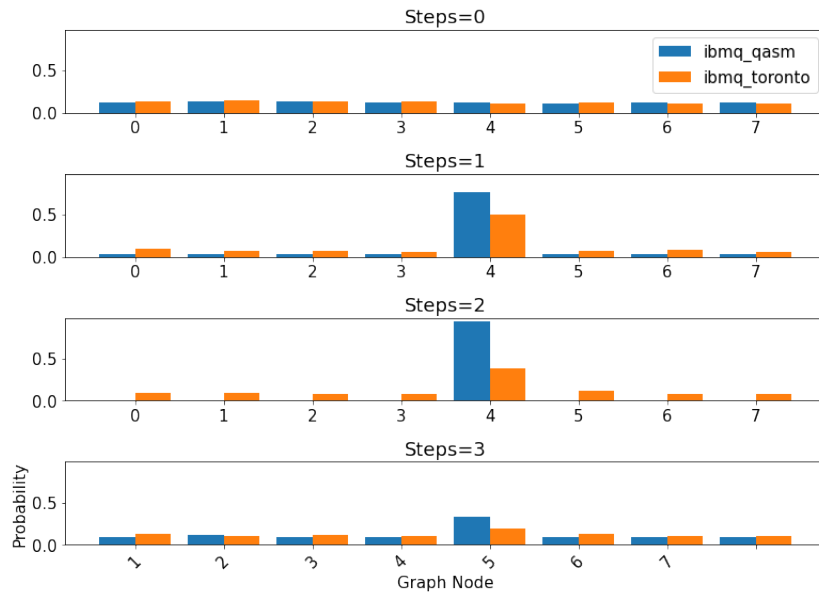


Figure 47: Probability distributions of the staggered quantum walk search problem for several steps, in a complete graph of size $N = 8$. The blue bar plot represents a circuit run in the QASM simulator, and the orange bar plot on IBM’s Toronto backend.

probability of the marked vertex was achieved in 1 step of the walk instead of the expected 2 steps, as in the Grover algorithm. Looking at the 1 step case in the simulator, one can see that the probability of vertex $|4\rangle$ is very close to the maximum, while the circuit has about half of the operations of the 2 step case. This means it is not surprising that the smaller circuit produces higher results for the probability of the marked vertex. For better context, the number of CNOT gates for 1, 2 and 3 steps were 18, 37 and 64, which is a big improvement when compared to the coined model.

This can be further confirmed by the fidelities of each of the states, which are approximately 0.954 and 0.780 for 1 and 2 steps, respectively. Thus, the former circuit produces better results because of the number of operations, even though that the latter should theoretically yield the highest probability.

Even though these results are a great improvement with respect to the algorithm using the coined quantum walk, the staggered model is still discrete, meaning its circuit will increase in depth as the number of steps increases. This can be avoided by turning again to the continuous-time quantum walk, whose circuit remains constant with time. However, to address the searching problem, the continuous-time model might not produce the best results, because it will need extra iterations due to the Suzuki-Trotter approximation and it will also require extra operations to implement the oracle, which was not the case in the pure dynamics example of section 4.3.

4.4.4 Searching with a Continuous-Time Quantum Walk

As seen in section 3.4, the unitary operator associated with the continuous time quantum walk model can be modified to mark an element for amplitude amplification

$$U'(t) = e^{iH't} = \phi(t)e^{-i(\gamma A+O)t}, \quad (127)$$

where $\phi(t)$ is a global phase, A is the adjacency matrix and the oracle defined as

$$O = \sum_{m \in M} |m\rangle \langle m|, \quad (128)$$

for M being the set of marked elements.

This section will focus on constructing and analyzing the circuit corresponding to the continuous-time quantum walk search problem, to be performed over a complete graph whose adjacency matrix is the following

$$A = \begin{pmatrix} 0 & 1 & \cdots & 1 & 1 \\ 1 & 0 & \cdots & 1 & 1 \\ \vdots & \vdots & \vdots & \vdots & \vdots \\ 1 & 1 & \cdots & 0 & 1 \\ 1 & 1 & \cdots & 1 & 0 \end{pmatrix}. \quad (129)$$

which is simply a matrix with all entries set to 1, except the diagonal.

The first step is to borrow the diagonal definition of the adjacency matrix from equation (109)

$$A = F^\dagger \Lambda F, \quad (130)$$

and use the Suzuki-Trotter expansion

$$e^{i(H_0+H_1)t} = \lim_{r \rightarrow \infty} (e^{i\frac{H_0t}{r}} e^{i\frac{H_1t}{r}})^r, \quad (131)$$

to decompose the operator in equation (127)

$$e^{i(\gamma A+O)t} = \lim_{r \rightarrow \infty} (F^\dagger e^{i\gamma\frac{\Lambda t}{r}} F e^{i\frac{O t}{r}})^r. \quad (132)$$

This can be easily translated into a circuit scheme as in figure 48.

Consider the case of a graph of size $N = 2^3 = 8$ and trotter number of $r = 1$. The corresponding Qiskit circuit is shown in figure 48. The system starts out in an uniform superposition followed by the application of the oracle operator as can be seen in figure 50.

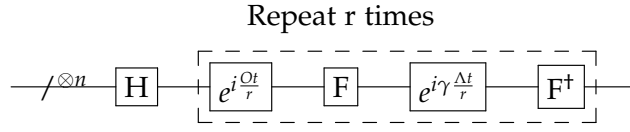


Figure 48: General circuit for the search problem using the continuous-time quantum walk model.

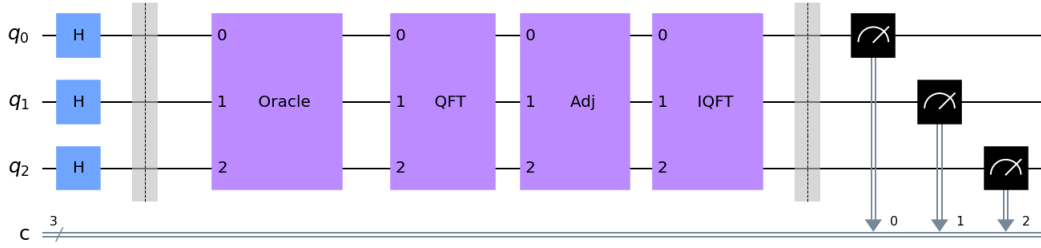


Figure 49: Qiskit circuit for the search problem using the continuous-time quantum walk model, for a complete graph of size $N = 8$, time t , a value of $\gamma = \frac{1}{8}$ and a Trotter number $r = 1$.

Note that the circuit was obtained with Qiskit’s *diagonal* function that takes the diagonal entries of the operator corresponding to the oracle defined in equation (132).

The next operation to be applied is the QFT but, because a complete graph is considered, the AQFT can be used with a degree of $m = 2$, which means the circuit will simply amount to Hadamard transforms, thus reducing its depth.

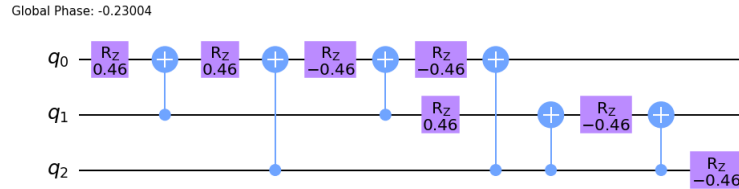


Figure 50: Qiskit circuit of the diagonal oracle operator in the continuous-time quantum walk search problem, for a complete graph of size $N = 8$, marked element $|m\rangle = |4\rangle$ and time $t = \frac{\pi}{2}\sqrt{8}$.

Then, the operator associated with the adjacency matrix is shown in figure 51. Since A is the diagonal adjacency matrix of a complete graph, it is easily implemented using the aforementioned *diagonal* function.

Finally, the results of circuit measurement can be seen in figure 52. Even though the circuit depth does not scale up with time, introducing the oracle operation to the continuous-time quantum walk model appears to make the circuit hard to run in a NISQ computer. For a single Trotter iteration, the number of CNOT gates was 37 for all times, which is slightly worse than 1 step of the staggered quantum walk.

Note that, theoretically, 2 iterations of the Suzuki-Trotter expansion are needed for maximum probability of the marked vertex to be achieved in optimal time. In practice, however,

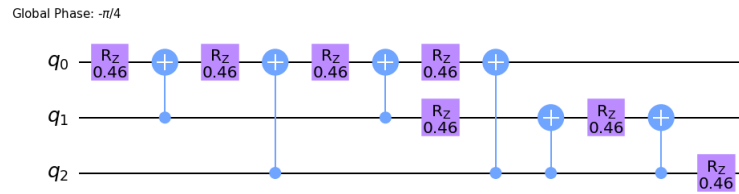


Figure 51: Qiskit circuit of the diagonal operator associated with the adjacency matrix in the continuous-time quantum walk search problem, for a complete graph of size $N = 8$, marked element $|m\rangle = |4\rangle$, time $t = \frac{\pi}{2}\sqrt{8}$ and $\gamma = \frac{1}{8}$.

greater probability for this element is achieved when only 1 iteration is performed since the smaller circuit seems to produce a greater fidelity of 0.71, when compared to a fidelity of 0.59 for the 2 iteration case. This is due to the fact that for $r = 2$, the number of CNOT gates increases to 77, which is approximately double than the $r = 1$ case.

The approximate quantum Fourier transform also has a positive impact, increasing fidelity from 0.60 when the full QFT circuit is used, to the aforementioned 0.71 when only Hadamard transformations are performed.

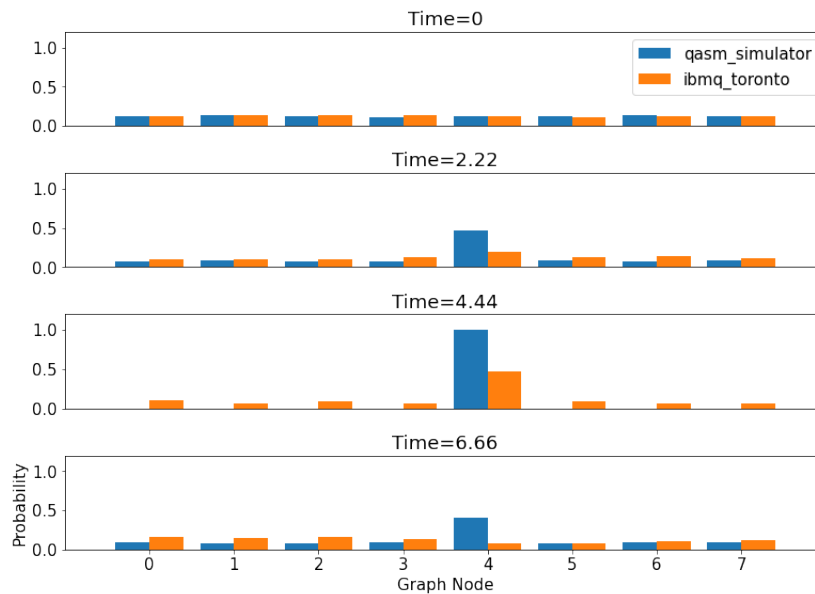


Figure 52: Probability distributions of the continuous-time quantum walk search problem for several time intervals, in a complete graph of size $N = 8$. The blue bar plot represents a circuit run in the QASM simulator, and the orange bar plot on IBM’s Toronto backend.

In conclusion, when comparing the different quantum walk models studied in previous sections, the coined quantum walk seems to be the least suited for supporting a search algorithm in NISQ computers. Then comes the continuous-time model which has the advantage of not scaling with time, but produces a circuit slightly too large to achieve a fidelity which rivals the staggered quantum walk. The latter appears to have the best

performance because, even though its discrete nature requires several iterations, the circuit depth does not appear to introduce a drastic amount of noise for the $N = 8$ case.

DISCUSSIONS AND CONCLUSION

Chapter 1 began with a brief historical overview of the origins of quantum computation, from the early days of Computer Science all the way to quantum walks. An overview of the state of the art encompassing both theoretical and circuit implementations of quantum walks and searching problems based on them was presented later, including the relevant literature for this thesis. This introduction is closed with an overview of the following chapters and main contributions.

The goal of the chapter 2 was to define the theoretical framework associated with the three quantum walk models studied in this thesis. This was done in the context of the quantum walk on the line, starting with a brief definition of the classical random walk, followed by the discrete models of the quantum walk, namely the coined model and the staggered model, and finishing with the continuous-time quantum walk. All the models were simulated in Python, and various plots were created in order to analyze how the different parameters influence the dynamics of each walk.

Chapter 3 was devoted to the study of the previously defined quantum walks when applied to the searching problem. It starts with the definition of the Grover algorithm and its complexity analysis, followed by the quantum walk analogue. The theoretical explanations for the various quantum walks on complete graphs were discussed, combined with the introduction of the oracle. As in the previous chapter, Python was used to simulate the algorithms and study how the different aspects of each model affect how the way the search algorithm evolves.

The main original contributions of this thesis are presented in chapter 4. The first contribution is a systematic way of creating Qiskit circuits implementing continuous-time quantum walks for a myriad of circulant graphs, resorting to the quantum Fourier transform and Qiskit's *diagonal* function, presented in the work by Santos et al. (2021) accepted in SBRC 2021 - WQuantum / Comunicação e Computação Quântica. Previous work by Qiang et al. (2016) uses the concept of circulant graphs for the implementation of the CTQW model on a complete graph for a small number of qubits. However this work provides a systematic way of generating circuits for a much greater number of circulant graphs, for an arbitrary number of qubits, as well as an analysis of how the approximate quantum Fourier transform

can be used to reduce circuit depth for better results in NISQ computers. Another original contribution, was the use of this method to implement search on circulant graphs resorting to the continuous-time quantum walk. The results were not as satisfactory as in the previous dynamics example, because of the increase in the circuit size due to the introduction of the oracle and Suzuki-Trotter iterations. This is still a work in progress, which will be further expanded upon in future publications. This chapter also contains a compilation of methods for creating circuits for the dynamics and search of the discrete-time quantum walk models, based mainly on the work of [Douglas \(2009\)](#) and [Acasiete et al. \(2020\)](#). These are not original contributions but hopefully provide a useful overview on how to implement these algorithms on current quantum hardware.

Based on what was achieved in this dissertation, future work for the study and implementation of quantum walks includes the following:

1. The circuit implementation of the continuous-time quantum walk search problem using circulant graphs, and the investigation on how the AQFT affects circuit depth and implementability on NISQ computers. This is the goal of a planned next publication.
2. Simulation, implementation and analysis of the searching problem for multiple marked elements using the staggered quantum walk model. The search problem with the SQW is not very well documented in the literature, with fundamental issues still lacking.
3. Analysis, through simulation of the continuous-time quantum walk, from the perspective of transport problems, such as localization, perfect state transfer and mixing time, and further analysis of the search problem for multiple marked elements.
4. Development of a method for constructing staggered quantum walk circuits for a larger variety of graphs.
5. Expansion of the circulant graph method for the CTQW in order to perform the walk over a larger class of graphs.

BIBLIOGRAPHY

- F. Acasiete, F. P. Agostini, J. Khatibi Moqadam, and R. Portugal. Implementation of quantum walks on ibm quantum computers. *Quantum Information Processing*, 19(12), Nov 2020. ISSN 1573-1332. doi: 10.1007/s11128-020-02938-5. URL <http://dx.doi.org/10.1007/s11128-020-02938-5>.
- Manindra Agrawal, Neeraj Kayal, and Nitin Saxena. Primes is in p. *Annals of Mathematics*, 160, 09 2002. doi: 10.4007/annals.2004.160.781.
- Dorit Aharonov, Andris Ambainis, Julia Kempe, and Umesh Vazirani. Quantum walks on graphs. *STOC '01 Proceedings of the thirty-third annual ACM symposium on Theory of computing*, pages 50–59, 2001.
- Dorit Aharonov, Wim van Dam, Julia Kempe, Zeph Landau, Seth Lloyd, and Oded Regev. Adiabatic quantum computation is equivalent to standard quantum computation. *SIAM Journal on Computing*, 37(1), 2007. doi: 166-194.
- Y. Aharonov, L. Davidovich, and N. Zagury. Quantum random walks. *Physical Review A*, 48(2):1687–1690, 1993.
- Andris Ambainis. Quantum walk algorithm for element distinctness. *SIAM Journal on Computing*, 37(1):210–239, 2007.
- Radhakrishnan Balu, Daniel Castillo, and George Siopsis. Physical realization of topological quantum walks on ibm-q and beyond. 2017.
- Adriano Barenco, Charles H. Bennett, Richard Cleve, David P. DiVincenzo, Norman Margolus, Peter Shor, Tycho Sleator, John A. Smolin, and Harald Weinfurter. Elementary gates for quantum computation. *Physical Review A*, 52(5):3457–3467, Nov 1995. ISSN 1094-1622. doi: 10.1103/physreva.52.3457. URL <http://dx.doi.org/10.1103/PhysRevA.52.3457>.
- Adriano Barenco, Artur Ekert, Kalle-Antti Suominen, and Päivi Törmä. Approximate quantum fourier transform and decoherence. *Physical Review A*, 54(1):139–146, Jul 1996. ISSN 1094-1622. doi: 10.1103/physreva.54.139. URL <http://dx.doi.org/10.1103/PhysRevA.54.139>.
- Paul Benioff. The computer as a physical system: A microscopic quantum mechanical hamiltonian model of computers as represented by turing machines. *Journal of Statistical Physics*, 22(5):563–591, 1980.

- Charles Bennett and Gilles Brassard. Withdrawn: Quantum cryptography: Public key distribution and coin tossing. *Theoretical Computer Science - TCS*, 560:175–179, 01 1984. doi: 10.1016/j.tcs.2011.08.039.
- Charles H. Bennett and Stephen J. Wiesner. Communication via one- and two-particle operators on einstein-podolsky-rosen states. *Phys. Rev. Lett.*, 69:2881–2884, Nov 1992. doi: 10.1103/PhysRevLett.69.2881. URL <https://link.aps.org/doi/10.1103/PhysRevLett.69.2881>.
- Scott D. Berry, Paul Bourke, and Jingbo B. Wang. qwviz: Visualisation of quantum walks on graphs. *Computer Physics Communications*, 182(10):2295–2302, 2011. ISSN 0010-4655. doi: <https://doi.org/10.1016/j.cpc.2011.06.002>. URL <https://www.sciencedirect.com/science/article/pii/S0010465511002128>.
- Michael Boyer, Gilles Brassard, Peter Høyer, and Alain Tapp. Tight bounds on quantum searching. *Fortschritte der Physik*, 46(4-5):493–505, 1998.
- A. R. Calderbank and Peter W. Shor. Good quantum error-correcting codes exist. *Phys. Rev. A*, 54:1098–1105, Aug 1996. doi: 10.1103/PhysRevA.54.1098. URL <https://link.aps.org/doi/10.1103/PhysRevA.54.1098>.
- D. Cheung. Improved bounds for the approximate qft. *Proc. of the Winter Intl Symposium of Information and Communication Technologies*, pages 192–197, 2004.
- Chen-Fu Chiang, Daniel Nagaj, and Pawel Wocjan. Efficient circuits for quantum walks. *Quantum Information and Computation*, 10, 03 2009. doi: 10.26421/QIC10.5-6-4.
- Andrew M. Childs. Universal computation by quantum walk. *Physical Review Letters*, 102 (18):180501, 2009.
- Andrew M. Childs and Jeffrey Goldstone. Spatial search by quantum walk. *Physical Review A*, 70(2):022314, 2004.
- Andrew M. Childs, Richard Cleve, Enrico Deott, Edward Farhi, Sam Gutmann, and Daniel A. Spielman. Exponential algorithmic speedup by quantum walk. *Proc. 35th ACM Symposium on Theory of Computing (STOC 2003)*, pp. 59-68, 2002. doi: 10.1145/780542.780552.
- Paul H. Cootner. *The random character of stock market prices*. M.I.T. Press, Cambridge, Mass, rev. ed. edition, 1967.
- D. Coppersmith. An approximate fourier transform useful for quantum factoring. Feb 2002.
- Gabriel Coutinho and Renato Portugal. Discretization of continuous-time quantum walks via the staggered model with hamiltonians. *Natural Computing*, pages 1–7, 2018.

- David Deutsch. Quantum theory, the church-turing principle and the universal quantum computer. *Proceedings of The Royal Society A Mathematical Physical and Engineering Sciences*, 400(1818), 1985.
- David Deutsch and Richard Jozsa. Rapid solution of problems by quantum computation. *Proceedings of The Royal Society A Mathematical Physical and Engineering Sciences*, 439(1907), 1992.
- B. Douglas. Efficient quantum circuit implementation of quantum walks. *Phys. Rev. A*, 79, 05 2009. doi: 10.1103/PhysRevA.79.052335.
- Martin Dyer, Alan Frieze, and Ravi Kannan. A random polynomial-time algorithm for approximating the volume of convex bodies. *Journal of the ACM*, 38(1):1–17, 1991.
- Matthew Falk. Quantum search on the spatial grid. 2013.
- Peter E. Falloon, Jeremy Rodriguez, and Jingbo B. Wang. Qswalk: A mathematica package for quantum stochastic walks on arbitrary graphs. *Computer Physics Communications*, 217: 162–170, 2017. ISSN 0010-4655. doi: <https://doi.org/10.1016/j.cpc.2017.03.014>. URL <https://www.sciencedirect.com/science/article/pii/S0010465517301029>.
- E. Farhi, J. Goldstone, S. Gutmann, and M. Sipser. Quantum computation by adiabatic evolution. *arXiv: Quantum Physics*, 2000.
- Edward Farhi and Sam Gutmann. An analog analogue of a digital quantum computation. *Physical Review A*, 57(4):2403–2406, 1998.
- Richard P. Feynman. There’s plenty of room at the bottom. *Feynman and computation*, pages 63–76, 1959.
- Richard P. Feynman. Simulating physics with computers. *International Journal of Theoretical Physics*, 21(6-7):467–488, 1982.
- Steven Finch. Pólya’s random walk constant. *Cambridge University Press*, pages 322–331, 2003.
- Konstantinos Georgopoulos and P. Zuliani. One-dimensional hadamard quantum walk on a cycle with rotational implementation. *arXiv: Quantum Physics*, 2019.
- Adam Glos, Jarosław Adam Miszczak, and Mateusz Ostaszewski. Qswalk.jl: Julia package for quantum stochastic walks analysis. *Computer Physics Communications*, 235:414–421, Feb 2018. ISSN 0010-4655. doi: 10.1016/j.cpc.2018.09.001. URL <http://dx.doi.org/10.1016/j.cpc.2018.09.001>.

- Geoffrey Grimmett, Svante Janson, and Petra F. Scudo. Weak limits for quantum random walks. *Physical Review E*, 69(2):026119, 2003.
- Lov K. Grover. A fast quantum mechanical algorithm for database search. *STOC '96 Proceedings of the twenty-eighth annual ACM symposium on Theory of computing*, pages 212–219, 1996.
- C. A. R. Hoare. Algorithm 64: Quicksort. *Commun. ACM*, 4(7):321, 1961. ISSN 0001-0782. doi: 10.1145/366622.366644. URL <https://doi.org/10.1145/366622.366644>.
- Norio Inui, Yoshinao Konishi, and Norio Konno. Localization of two-dimensional quantum walks. *Physical Review A*, 69(5):052323, 2003.
- Josh Izaac and Jb Wang. Pyctqw: A continuous-time quantum walk simulator on distributed memory computers. *Computer Physics Communications*, 186, 01 2015. doi: 10.1016/j.cpc.2014.09.011.
- Mark Jerrum, Alistair Sinclair, and Eric Vigoda. A polynomial-time approximation algorithm for permanent of a matrix with nonnegative entries. *Journal of the ACM*, 51(4):671–697, 2004.
- Norio Konno. A new type of limit theorems for the one-dimensional quantum random walk. *J. Math. Soc. Japan*, 57(4):1179–1195, 2002.
- A. Lenstra, H. Lenstra, M. Manasse, and J. Pollard. The number field sieve. pages 564–572, 01 1990. doi: 10.1145/100216.100295.
- T Loke and J B Wang. Efficient quantum circuits for continuous-time quantum walks on composite graphs. *Journal of Physics A: Mathematical and Theoretical*, 50(5):055303, Jan 2017a. ISSN 1751-8121. doi: 10.1088/1751-8121/aa53a9. URL <http://dx.doi.org/10.1088/1751-8121/aa53a9>.
- T. Loke and J.B. Wang. Efficient quantum circuits for szegedy quantum walks. *Annals of Physics*, 382:64–84, Jul 2017b. ISSN 0003-4916. doi: 10.1016/j.aop.2017.04.006. URL <http://dx.doi.org/10.1016/j.aop.2017.04.006>.
- Neil B. Lovett, Sally Cooper, Matthew Everett, Matthews Trevers, and Viv Kendon. Universal quantum computation using the discrete quantum walk. *Physical Review A*, 81(4):042330, 2010.
- Frédéric Magniez, Ashwin Nayak, Jérémie Roland, and Miklos Santha. Search via quantum walk. *SIAM Journal on Computing*, 40(1):142–164, 2006.
- Frédéric Magniez, Miklos Santha, and Mario Szegedy. Quantum algorithms for the triangle problem. *SIAM Journal on Computing*, 37(2):413–424, 2007.

- F.L. Marquezino and R. Portugal. The qwalk simulator of quantum walks. *Computer Physics Communications*, 179(5):359–369, Sep 2008. ISSN 0010-4655. doi: 10.1016/j.cpc.2008.02.019. URL <http://dx.doi.org/10.1016/j.cpc.2008.02.019>.
- Dmitri Maslov. Advantages of using relative-phase toffoli gates with an application to multiple control toffoli optimization. *Physical Review A*, 93(2), Feb 2016. ISSN 2469-9934. doi: 10.1103/physreva.93.022311. URL <http://dx.doi.org/10.1103/PhysRevA.93.022311>.
- Elliott Montroll. Random walks in multidimensional spaces, especially on periodic lattices. *Journal of the Society for Industrial and Applied Mathematics*, 4(4):241–260, 1956. doi: 10.1137/0104014.
- Elliott Waters Montroll and George Herbert Weiss. Random walks on lattices. ii. *Journal of Mathematical Physics*, page 167–181, 1997.
- Gordon E. Moore. Cramming more components onto integrated circuits. *Electronics*, 38(8): 114–117, 1965.
- J.K. Moqadam, M. C. de Oliveira, and Renato Portugal. Staggered quantum walks with superconducting microwave resonators. *Physical Review B*, 95(14):144506, 2017.
- Rajeev Motwani and Prabhakar Raghavan. *Randomized Algorithms*. Cambridge University Press, 1995.
- Ashwin Nayak and Ashvin Vishwanath. Quantum walk on the line. 2000.
- Michael A. Nielsen and Isaac L. Chuang. *Quantum Computation and Quantum Information: 10th Anniversary Edition*. Cambridge University Press New York, NY, USA, 2011.
- Christos Papadimitriou. *Computational Complexity*. Pearson, 1994.
- Apoorva Patel, K.S. Raghunathan, and Pranaw Rungta. Quantum random walks do not need a coin toss. *Physical Review A*, 71(3):032347, 2005.
- Karl Pearson. The problem of the random walk. *Nature*, 72(1865):294, 1905. doi: 10.1038/072294bo.
- R. Portugal, R.A.M. Santos, T.D. Fernandes, and D.N. Goncalves. The staggered quantum walk model. *Quantum Information Processing*, 15(1):85–101, 2016.
- Renato Portugal. Establishing the equivalence between szegedy’s and coined quantum walks using the staggered model. *Quantum Information Processing*, 15(4):1387–1409, 2015.
- Renato Portugal. *Quantum Walks and Search Algorithms*. Springer, 2018.

- Renato Portugal and T. D. Fernandes. Quantum search on the two-dimensional lattice using the staggered model with hamiltonians. *Physical Review A*, 95(4):042341, 2017.
- Renato Portugal, Stefan Boettcher, and Stefan Falkner. One-dimensional coinless quantum walks. *Physical Review A*, 91(5):052319, 2015.
- Renato Portugal, M. C. de Oliveira, and J. K. Moqadam. Staggered quantum walks with hamiltonians. *Physical Review A*, 95(1):012328, 2017.
- George Pólya. Über eine aufgabe der wahrscheinlichkeitsrechnung betreffend die irrfahrt im straßennetz. *Mathematische Annalen*, 84:149–160, 1921. doi: 10.1007/BF01458701.
- Xiaogang Qiang, Thomas Loke, Ashley Montanaro, Kanin Aungskunsiri, Xiaoqi Zhou, Jeremy L. O’Brien, Jingbo B. Wang, and Jonathan C. F. Matthews. Efficient quantum walk on a quantum processor. *Nature Communications*, 7(1), May 2016. ISSN 2041-1723. doi: 10.1038/ncomms11511. URL <http://dx.doi.org/10.1038/ncomms11511>.
- J. J. Sakurai. *Modern Quantum Mechanics*. Addison-Wesley Publishing, Co, 1994.
- Miklos Santha. Quantum walk based search algorithms. *International Conference on Theory and Applications of Models of Computation. TAMC 2008. Lecture Notes in Computer Science*, 4978:31–46, 2008.
- J. Santos, B. Chagas, and R. Chaves. Quantum walks on a superconducting quantum computer. *Simpósio Brasileiro de Redes de Computadores e Sistemas Distribuídos*, July 2021.
- Marek Sawerwain and Roman Gielerek. Gpgpu based simulations for one and two dimensional quantum walks. *Communications in Computer and Information Science*, page 29–38, 2010. ISSN 1865-0937. doi: 10.1007/978-3-642-13861-4-3. URL <http://dx.doi.org/10.1007/978-3-642-13861-4-3>.
- Benjamin Schumacher. Quantum coding. *Phys. Rev. A*, 51:2738–2747, Apr 1995. doi: 10.1103/PhysRevA.51.2738. URL <https://link.aps.org/doi/10.1103/PhysRevA.51.2738>.
- Uwe Schöning. A probabilistic algorithm for k-sat and constraint satisfaction problems. *40th Annual Symposium on Foundations of Computer Science*, pages 410–, 1999.
- Asif Shakeel. Efficient and scalable quantum walk algorithms via the quantum fourier transform. *Quantum Information Processing*, 19(9), Aug 2020. ISSN 1573-1332. doi: 10.1007/s11128-020-02834-y. URL <http://dx.doi.org/10.1007/s11128-020-02834-y>.
- C. E. Shannon. A mathematical theory of communication. *The Bell System Technical Journal*, 27(3):379–423, 1948. doi: 10.1002/j.1538-7305.1948.tb01338.x.

- V.V. Shende, S.S. Bullock, and I.L. Markov. Synthesis of quantum-logic circuits. *IEEE Transactions on Computer-Aided Design of Integrated Circuits and Systems*, 25(6):1000–1010, Jun 2006. ISSN 1937-4151. doi: 10.1109/tcad.2005.855930. URL <http://dx.doi.org/10.1109/TCAD.2005.855930>.
- Neil Shenvi, Julia Kempe, and Birgitta Whaley. A quantum random walk search algorithm. *Physical Review A*, 67(5):052307, 2003.
- Peter W. Shor. Algorithms for quantum computation: Discrete logarithms and factoring. *Proceedings 35th Annual Symposium on Foundations of Computer Science*, pages 124–134, 1994a.
- P.W. Shor. Algorithms for quantum computation: discrete logarithms and factoring. *Proceedings 35th Annual Symposium on Foundations of Computer Science*, pages 124–134, 1994b. doi: 10.1109/SFCS.1994.365700.
- Alexander Slepoy. Quantum gate decomposition algorithms. *Sandia National Laboratories*, 2006.
- R. Solovay and V. Strassen. A fast monte-carlo test for primality. *SIAM Journal on Computing*, 6(1):84–85, 1977. doi: 10.1137/0206006. URL <https://doi.org/10.1137/0206006>.
- Tommi Sottinen. Fractional brownian motion, random walks and binary market models. *Finance and Stochastics*, (5):343–355, 2001. doi: 10.1007/PL00013536.
- Andrew Steane. Multiple-particle interference and quantum error correction. *Proceedings of the Royal Society of London. Series A: Mathematical, Physical and Engineering Sciences*, 452(1954):2551–2577, 1996. doi: 10.1098/rspa.1996.0136. URL <https://royalsocietypublishing.org/doi/abs/10.1098/rspa.1996.0136>.
- Mario Szegedy. Quantum speed-up of markov chain based algorithms. *45th Annual IEEE Symposium on Foundations of Computer Science*, 2004.
- Alan Turing. On computable numbers, with an application to the entscheidungsproblem. *Proceedings of the London Mathematical Society*, s2-42(1):230–265, 1936.
- Salvador Elías Venegas-Andraca. Quantum walks: a comprehensive review. *Quantum Information Processing*, 11(5):1015–1106, 2012.
- J. von Neumann. First draft of a report on the edvac. *IEEE Annals of the History of Computing*, 15(4):27–75, 1993. doi: 10.1109/85.238389.
- Stephen Wiesner. Conjugate coding. *SIGACT News*, 15(1):78–88, 1983. ISSN 0163-5700. doi: 10.1145/1008908.1008920. URL <https://doi.org/10.1145/1008908.1008920>.

Christof Zalka. Grover's quantum searching algorithm is optimal. *Physical Review A*, 60(4): 2746–2751, 1999.



SUPPORT MATERIAL

A.1 THE POSTULATES OF QUANTUM MECHANICS

Quantum mechanics, firstly discovered in the decade of 1920, is a mathematical framework for developing physical theories. This section revisits the basic postulates of quantum mechanics, which are formalized resorting to the Dirac notation. Further reading on this notation includes the work of [Sakurai \(1994\)](#) and, for an extensive review of quantum computation, the book by [Nielsen and Chuang \(2011\)](#).

The first postulate defines where the processes of quantum mechanics take place. The *state* of a system describes its physical characteristics, so some rules are required for these mathematical objects to have a connection to the real world.

Postulate 1 (State Space) *Any isolated physical system has an associated Hilbert Space, \mathcal{H} , known as the state space. The state of the system is wholly described by its state vector $|\psi\rangle \in \mathcal{H}$. The physical system's degrees of freedom dictate the dimension of \mathcal{H}*

Note that this postulate does not tell us the Hilbert space of any given physical system, nor does it tell us its state vector. It is generally hard to define the Hilbert space of an arbitrary system, which makes the work physicists have done in developing certain theories, like quantum electrodynamics, even more remarkable.

Considering the computational basis $\{|0\rangle, |1\rangle\}$, the simplest quantum system, the *qubit*, can be defined as

$$|\psi\rangle = \alpha |0\rangle + \beta |1\rangle, \quad (133)$$

where α, β are complex numbers and

$$|0\rangle = \begin{pmatrix} 1 \\ 0 \end{pmatrix} \quad \text{and} \quad |1\rangle = \begin{pmatrix} 0 \\ 1 \end{pmatrix}. \quad (134)$$

Because Hilbert spaces are also vector spaces, linear combinations of these states are also allowed

$$|\psi\rangle = \sum_i \alpha_i |\varphi_i\rangle. \quad (135)$$

Since $|\psi\rangle$ is required to be a unit vector, $|\psi\rangle\langle\psi| = 1$ or, equivalently,

$$\sum_j |\alpha_j|^2 = 1. \quad (136)$$

These combinations, known as *superpositions*, are the main difference between a classical bit and a qubit, where the states are not in a definite value before measurement. This is a well studied quantum phenomenon that leads to constructive and destructive interference between states, which is an aspect many algorithms indeed exploit.

The second postulate aims to describe how a quantum system evolves with time, and it can be formulated in the following way.

Postulate 2 (Evolution) *The time evolution of a closed quantum system is described by a unitary operator. Considering an initial condition $|\psi_0\rangle$, then for any time evolution of a closed quantum system, a unitary operator U exists such that $|\psi_f\rangle = U|\psi_0\rangle$.*

Just as the first postulate does not specify a Hilbert space, the evolution postulate does not state which unitary operators U describe an arbitrary physical system. What it does state is that the evolution of a closed quantum system follows those rules. More specifically, the second postulate describes the dynamics of such systems. In the case of a qubit, any U can be performed in a realistic system as long as $UU^\dagger = U^\dagger U = I$, which is another way of saying that U is unitary.

There are a number of unitary operators very relevant to quantum computation, known as *Pauli matrices*, that are usually composed to create more general matrices. These are defined as

$$I = \begin{pmatrix} 1 & 0 \\ 0 & 1 \end{pmatrix}, \quad X = \begin{pmatrix} 0 & 1 \\ 1 & 0 \end{pmatrix}, \quad Y = \begin{pmatrix} 0 & -i \\ i & 0 \end{pmatrix} \quad \text{and} \quad Z = \begin{pmatrix} 1 & 0 \\ 0 & -1 \end{pmatrix}. \quad (137)$$

Postulate 2 tells us the relationship between the states of the system at two different times. An improved version of this postulate takes time as a continuous variable, stating that the temporal evolution of a closed quantum system can be described by the Schrodinger equation

$$i\hbar \frac{d|\psi\rangle}{dt} = H|\psi\rangle, \quad (138)$$

where \hbar is the *Planck's constant* and H is a Hermitian operator known as the *Hamiltonian* of the system. In principle, the Hamiltonian can be used to describe a system in its entirety. However figuring out the Hamiltonian is generally a hard task.

So far only single quantum systems have been considered. The next postulate describes how one can create composite quantum systems made of smaller distinct systems.

Postulate 3 (Composite Systems) *The state space of a system composed of smaller sub-systems can be described by the tensor product of the individual state spaces $\mathcal{H}_1 \otimes \mathcal{H}_2$. Moreover, if the first system's state is $|\psi_1\rangle$ and the second is $|\psi_2\rangle$ then the state of the composite system is $|\psi_1\rangle \otimes |\psi_2\rangle$.*

The tensor product is used because of the nature of superposition in quantum mechanics. A system composed of subsystems $\{|\psi\rangle, |\varphi\rangle\}$ is denoted as $|\psi\rangle \otimes |\varphi\rangle$. Recalling the superposition principle, that tells us that any complex linear combination of states belonging to the system is also allowed, the tensor product naturally follows.

The tensor notation can be written in a more compact way. A system described by n component states

$$|\psi\rangle = |\psi_0\rangle \otimes |\psi_1\rangle \otimes \cdots \otimes |\psi_{n-1}\rangle, \quad (139)$$

can be rewritten as

$$|\psi\rangle = |\psi_0\rangle |\psi_1\rangle \cdots |\psi_{n-1}\rangle, \quad (140)$$

and even further compacted to

$$|\psi\rangle = |\psi_0 \psi_1 \cdots \psi_{n-1}\rangle. \quad (141)$$

However, not all composite systems can be described as the tensor product of the component states. For example, state

$$|\psi\rangle = \frac{|00\rangle + |11\rangle}{\sqrt{2}}, \quad (142)$$

cannot be broken down further. These subsystems are known to be *entangled*, and the state in equation (142) is called a *Bell state*. Bell states describe the set of 2 qubit states that present maximum entanglement. They are used in many quantum applications like *quantum teleportation* and *superdense coding*.

As was mentioned above, closed quantum systems evolve unitarily in time. However, in order to do something useful with such a system, one must extract the underlying classical information. This is achieved by the process of measurement, which requires some form of interaction with the system, thus making it no longer closed nor described by a unitary evolution.

Postulate 4 (Measurement) *Quantum measurements are described by a set, $\{M_m\}$, of measurement operators that act on the state space of the system, satisfying the completeness relation $\sum_m M_m^\dagger M_m = I$, where m refers to the measurement outcomes. Considering a system with state $|\psi\rangle$, immediately before measurement, then the probability of an outcome m is*

$$p(m) = \langle \psi | M_m^\dagger M_m | \psi \rangle. \quad (143)$$

The state of the system after the measurement will be

$$|\psi'\rangle = \frac{1}{\sqrt{p(m)}} M_m |\psi\rangle. \tag{144}$$

Measurement can be done and interpreted in several different ways, however this appendix focuses on what is called *projective* measurement. A projective measurement is described by an Hermitian operator, M , known as an *observable*, with spectral decomposition

$$M = \sum_m m P_m \tag{145}$$

where P_m is an Hermitian projection operator with eigenvalue m . For example, P_1 and P_2 are projection operators that are orthogonal to each other and whose product is a zero matrix. A set of operators with these characteristics obey the completeness equation

$$\sum_i P_i = I. \tag{146}$$

The probability of outcome m associated with the measurement of state $|\psi\rangle$ can be written as

$$p(m) = \langle\psi| P_m |\psi\rangle. \tag{147}$$

Knowing that m was the result of the measurement, the resulting state for the quantum system is then

$$\frac{P_m}{\sqrt{p(m)}} |\psi\rangle. \tag{148}$$

An important case of projective measurement arises when it is performed in the *computational basis* of a qubit. Given operators

$$M_0 = |0\rangle\langle 0| = \begin{pmatrix} 1 & 0 \\ 0 & 0 \end{pmatrix} \text{ and } M_1 = |1\rangle\langle 1| = \begin{pmatrix} 0 & 0 \\ 0 & 1 \end{pmatrix}, \tag{149}$$

it is obvious that they are Hermitian and that they obey the completeness relation. Consider again the state $|\psi\rangle = \alpha |0\rangle + \beta |1\rangle$. The probability of outcome 0 will be

$$p(0) = \langle\psi| M_0^\dagger M_0 |\psi\rangle = \langle\psi| M_0 |\psi\rangle = |\alpha|^2 \tag{150}$$

and outcome 1

$$p(1) = \langle\psi| M_1^\dagger M_1 |\psi\rangle = \langle\psi| M_1 |\psi\rangle = |\beta|^2. \tag{151}$$

For each of the outcomes, the state after measurement will be

$$\frac{M_0}{|\alpha|} |\psi\rangle = \frac{\alpha}{|\alpha|} |0\rangle, \tag{152}$$

$$\frac{M_1}{|\beta|} |\psi\rangle = \frac{\beta}{|\beta|} |1\rangle. \tag{153}$$

Projective measurement destroys the superposition of possible states. This is known as the *collapse of the wave function*.

A.2 QUANTUM FOURIER TRANSFORM

As was seen in section 3.1, quantum computers can perform certain tasks more efficiently than classical ones. A well known such example is the problem of finding the prime factorization of an n -bit integer, which the most efficient solution to date, proposed by [Lenstra et al. \(1990\)](#), requires $e^{O(n^{\frac{1}{3}} \log^{\frac{2}{3}} n)}$ operations. In contrast, a quantum algorithm proposed by [Shor \(1994b\)](#) accomplishes the same task in $O((\log n)^2 (\log \log n) (\log \log \log n))$ operations, which amounts to an exponential gain due to the efficiency of the quantum Fourier transform.

The quantum Fourier transform is an implementation of the discrete Fourier transform over amplitudes of quantum states. It offers no speed ups when used in computing Fourier transforms of classical data, since the amplitudes cannot be accessed directly by measurement. Moreover, it is not known of a generalized, efficient way of preparing the initial state to be Fourier Transform. This means that the relevance of the QFT is not to provide a straightforward way of calculating discrete Fourier transforms, but to design algorithms, such as *phase estimation*, that take advantage of its properties. The QFT can be described as the following operation over an orthonormal basis $|0\rangle, |1\rangle, \dots, |N-1\rangle$

$$QFT(|j\rangle) = \frac{1}{\sqrt{N}} \sum_{k=0}^{N-1} e^{\frac{2\pi ijk}{N}} |k\rangle, \tag{154}$$

where $N = 2^n$. With a little bit of algebra, this can be rewritten as a product

$$\begin{aligned} \frac{1}{\sqrt{N}} \sum_{k=0}^{N-1} e^{\frac{2\pi ijk}{2^n}} |k\rangle &= \frac{1}{\sqrt{N}} \sum_{k_1=0}^1 \dots \sum_{k_n=0}^1 e^{2\pi i j (\sum_{l=1}^n k_l 2^{-l})} |k_1 \dots k_n\rangle \\ &= \frac{1}{\sqrt{N}} \bigotimes_{l=1}^n \left(\sum_{k_l=0}^1 e^{2\pi i j k_l 2^{-l}} |k_l\rangle \right) \\ &= \frac{1}{\sqrt{N}} \bigotimes_{l=1}^n (|0\rangle + e^{2\pi i j 2^{-l}} |1\rangle). \end{aligned} \tag{155}$$

The quantum Fourier transform applied to a state as in equation (154) can then be rewritten as

$$QFT(|x_1, \dots, x_n\rangle) = \frac{(|0\rangle + e^{2\pi i 0.x_n} |1\rangle)(|0\rangle + e^{2\pi i 0.x_{n-1}x_n} |1\rangle) \dots (|0\rangle + e^{2\pi i 0.x_1x_2 \dots x_n} |1\rangle)}{2^{\frac{N}{2}}}, \quad (156)$$

where $x = x_12^{n-1} + x_22^{n-2} + \dots + x_n2^0$ and the notation $0.x_1x_{l+1} \dots x_n$ represents the binary fraction $\frac{x_l}{2^{l^0}} + \frac{x_{l+1}}{2^1} \dots \frac{x_m}{2^{m-l+1}}$. This is a very useful representation because it makes constructing an efficient circuit much simpler, as can be seen in figure 53. However, the circuit implementation of the QFT requires exponentially smaller phase-shift gates as the number of qubits increases. This can be somehow mitigated by eliminating the smaller phase-shift gates at the cost of some accuracy, as was shown in Coppersmith (2002) who defined the *approximate* quantum Fourier transform. This approximation requires only $O(n \log n)$ gates. The work of Barenco et al. (1996) and Cheung (2004) established lower bounds for the probability of the approximate state accurately representing the state without approximation.

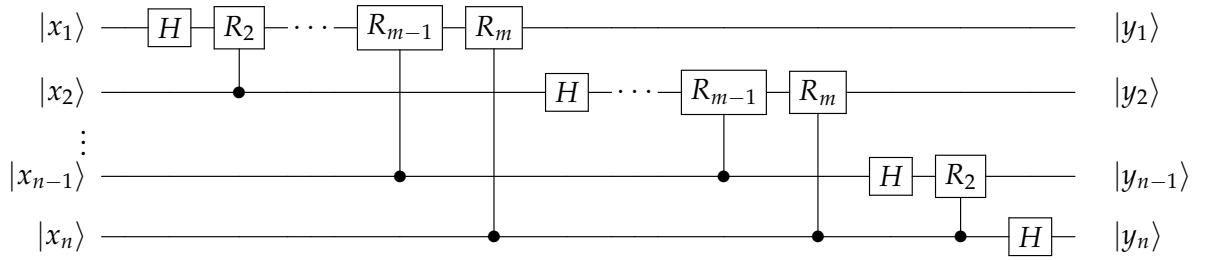


Figure 53: General circuit for the quantum Fourier transform.

The rotation R_k in figure 53 is defined as the controlled version of

$$R_k = \begin{pmatrix} 1 & 0 \\ 0 & e^{\frac{2\pi i}{2^k}} \end{pmatrix}. \quad (157)$$

To verify that this circuit is the QFT, consider the state $|x_1 \dots x_n\rangle$ as input. Applying the Hadamard gate on the first qubit produces the state

$$H |x_1 \dots x_n\rangle = \frac{1}{\sqrt{N}}(|0\rangle + e^{2\pi i 0.x_1} |1\rangle) |x_1 \dots x_n\rangle. \quad (158)$$

The next operation is the rotation R_2 , controlled by the second qubit, resulting in state

$$\frac{1}{\sqrt{N}}(|0\rangle + e^{2\pi i 0.x_1x_2} |1\rangle) |x_1 \dots x_n\rangle. \quad (159)$$

Applying the successive rotations up to R_n appends an extra bit to the phase of the first $|1\rangle$, ultimately becoming

$$\frac{1}{\sqrt{N}}(|0\rangle + e^{2\pi i 0.x_1 x_2 \dots x_n} |1\rangle) |x_1 \dots x_n\rangle. \quad (160)$$

A similar process is applied to the second qubit. At the end, the state has become

$$\frac{1}{\sqrt{N}}(|0\rangle + e^{2\pi i 0.x_1 x_2 \dots x_n} |1\rangle)(|0\rangle + e^{2\pi i 0.x_2 \dots x_n} |1\rangle) |x_1 \dots x_n\rangle, \quad (161)$$

and the successive application of this process to the remaining qubits results in state

$$\frac{1}{\sqrt{N}}(|0\rangle + e^{2\pi i 0.x_1 x_2 \dots x_n} |1\rangle)(|0\rangle + e^{2\pi i 0.x_2 \dots x_n} |1\rangle) \dots (|0\rangle + e^{2\pi i 0.x_n} |1\rangle) |x_1 \dots x_n\rangle, \quad (162)$$

confirming that this is indeed the Fourier transform derived in equation (156) up to the order of the qubits, which is reversed. It also shows that the QFT is unitary, since all operations in the circuit are unitary.

Counting the number of gates on the circuit, one can conclude that the first qubit will have 1 Hadamard gate followed by $n - 1$ controlled rotations. The second qubit is another Hadamard followed by $n - 2$ controlled rotations. After n qubits, the total number of gates will be $\frac{n(n+1)}{2}$. This means the circuit provides a $O(n^2)$ algorithm, compared to the fastest classical algorithm, the *Fast Fourier Transform*, which requires $O(n2^n)$ operations. This is an exponential gain, which can be improved upon at the cost of accuracy.